Thermophysical Properties of Natural Gas Components: Apparatus and Speed of Sound in Argon†

Anthony R. H. Goodwin*,‡ and James A. Hill

Center for Applied Thermodynamic Studies, College of Engineering, University of Idaho, Moscow, Idaho 83843

An apparatus consisting of two spherical resonators of nominal internal radius (25 and 45) mm was constructed and used to determine the speed of sound in argon at temperatures between (250 and 350) K at pressures below 7 MPa. The estimated expanded uncertainty in the speed of sound determined was less than ± 0.03 $m \cdot s^{-1}$, that is, $< \pm 8 \cdot 10^{-5} \cdot u$, and the results obtained from both resonators agreed within the combined uncertainty. Independent measurements and predictions, obtained from an equation of state (*J. Phys. Chem. Ref. Data* **1999**, *28*, 779−850), of the speed of sound differed from the results by $< \pm 5 \cdot 10^{-5} \cdot u$ at $p < 2.5$ MPa and at $p \approx 6.8$ MPa by $4 \cdot 10^{-4} \cdot u$. The second acoustic virial coefficient for argon obtained from both resonators agrees within the combined expanded uncertainty except at $T = 350$ K where the difference is about three times the combined expanded error.

Introduction

Natural gas is a mixture of predominantly methane combined with other hydrocarbons and nonhydrocarbons, such as N_2, CO_2, and H_2O(g). Natural gas is extracted from subterranean strata, gathered, processed, and transmitted, ultimately through distribution systems, to end users over a wide range of temperatures and pressures over which there is the opportunity to encounter phase boundaries. The propensity of natural gas to produce a liquid phase can give rise to errors in flow measurement and the production of unmarketable aromatics and thus the deterioration of storage facilities, pipeline corrosion, and degradation of the energy content of the gas.

The energy content is perhaps the most important from this list and certainly has an immediate impact on business because natural gas is sold by energy content and is typically metered by volume. The conversion between volume and energy requires the acquisition of a sample and either direct measurement of the enthalpy of combustion or indirect determination of the energy from measurements of the chemical composition combined with a thermodynamic database. The energy content of the gas can also be determined by methods known as inferential sensing that, in general, require an equation of state to relate the measurements to the desired quantity. This approach is an extension of the principle of the so-called sGERG equation of state[1] that uses three input properties to characterize the natural gas quality: calorific value, density at a reference condition, and the mole fraction of carbon dioxide. Jaeschke et al.[2] reported that the energy content could be determined from measurements of CO_2 mole fraction, ultimately providing information about the diluent content, speed of sound, and the relative electric permittivity; this included work performed by Ruhrgas, Gasunie, and GERG (Groupe Européen de Recherches Gazières).[3] As part of this effort Moldover and Buckley[4] determined reference values for the dielectric constant or relative electric permittivity of natural gas components. The mole fraction of CO_2 can be detected by infrared absorption spectroscopy at wavelengths in the range of (4.17 to 4.46) μm.

This article reports work sponsored by the Gas Research Institute (GRI) under contract number 5093-260-2599 that commenced in 1993. The project was charged to provide the experimental methods and fundamental data to permit in situ real-time determination of phase borders and energy content of natural gas by inferential sensing using measurements of the speed of sound and relative electric permittivity;[5,6] the latter can also provide (p, T) phase borders at constant composition.

The techniques chosen to determine sound speed and relative electric permittivity rely on the measurements of frequency, f, one of the most accurate ($\Delta f/f < 1 \cdot 10^{-8}$) and easily reproduced physical quantities. The intent of the apparatus was to provide, when all components were installed, simultaneous measurement of the following thermophysical properties of the fluid:[5,7,8] (1) location of the phase boundary (p, ρ, T, x), (2) relative permittivity, ε, (3) speed of sound, $u(T, p)$, and (4) molar perfect-gas heat capacity at constant pressure, $C_{p,m}^{pg}(T)$. Methods discussed in refs 9 and 10 can, when initial conditions of Z and $(\partial Z/\partial T)_p$ are known along the same isentropic path, be used to obtain the compression factor, $Z(T, p)$, and molar heat capacity at constant pressure, $C_{p,m}(T, p)$, from $u(T, p)$ measurements; the independent variables of (T, ρ_n), where ρ_n is the amount-of-substance density, can also be used with $u(T, p)$ as input.[9]

The aim of this article is to describe the two spherical acoustic resonators and present results for argon obtained over three years from 1994 through 1997[5,6] solely for the purpose of instrument validation.[11] Two resonators of different surface area to volume ratios can, when operated with the same gas, be used to reveal acoustic perturbations such as the effects of precondensation[12] and provide sound speed, when appropriately interconnected (p, V_m, T) from Burnett expansions.[13,14]

In future articles results for hydrocarbon gases, of greater technical significance,[11] will be presented as will details of the methods used to determine relative electric permittivity and phase border that have been outlined elsewhere[8] and are similar to those discussed by Moldover et al.,[15] Goodwin et al.,[16] and

† Part of the "William A. Wakeham Festschrift".

* To whom correspondence should be addressed. E-mail: agoodwin@slb.com or goodwin@jced.acs.org. Fax: +1 281-565-9658.

‡ Present address: Schlumberger Technology Corporation, 125 Industrial Boulevard, Sugar Land, Texas 77478.

10.1021/je900428g CCC: $40.75
Published on Web 09/10/2009

Goodwin and Moldover,[17] albeit less advanced than the instruments reported by either Kandil et al.[18−20] or May et al.[21]

Working Equations and Analysis

The virtues of spherical acoustic resonators for determining the speed of sound in gases have been reported by Moldover and co-workers,[22−28] Trusler,[29] and Goodwin and Trusler.[9,30] Indeed, measurement of the speed of sound is a convenient and accurate route for determining the heat capacity of polyatomic gases with sources of error that differ markedly from those encountered in conventional calorimetry.[30,31] The principle advantage of a spherical resonator for the determination of sound speed is the presence of radial modes because of both the absence of viscous damping at the surface and the insensitivity of the frequency to geometric imperfections.[32−35] For radial modes, only the internal volume of the cavity is required to determine the sound speed with a relative uncertainty of 10^{-6} from knowledge of the average radius $\langle a \rangle$; fluctuations of the radius over the surface of relative uncertainty of the order 10^{-3} can be permitted so that the resonator can be constructed without recourse to special machining methods. The absence of viscous damping and the favorable volume-to-surface ratio in the sphere lead to resonance quality factors in gases that are greater than attainable with any other geometry of similar volume and operating frequency.

The measured resonance frequencies $f_{0,n}(T, p)$ of the radial modes were analyzed according to the acoustic model, described elsewhere,[9,23−30,36] in which the ratio of the speed of sound $u(T, p)$ to resonator radius $a(T, p = 0)$ is given by

$$\frac{u(T,p)}{a(T,p=0)} = \{2\pi a(T,p)[f_{0,n}(T,p) - \sum_{\mathrm{j}} \Delta f_{\mathrm{j}}]/a(T,p=0)\}\nu_{0,n} \quad (1)$$

In eq 1, $a(T, p)$ is the radius at temperature T and pressure p, $a(T, p = 0)$ the radius at zero pressure, $\nu_{0,n}$ an eigenvalue for the radial modes for which $n = 1, 2, 3, ...$, and $\sum_{\mathrm{j}}\Delta f_{\mathrm{j}}$ the sum of j-th perturbations that accommodate energy loss.[9,23−30,36]

In eq 1 the $\sum_{\mathrm{j}}\Delta f_{\mathrm{j}}$ is given by

$$\sum_{\mathrm{j}} \Delta f_{\mathrm{j}} = (\Delta f_{\mathrm{th}} + \Delta f_{\mathrm{s}} + \Delta f_{\mathrm{o}} + \Delta f_{\mathrm{slot}}) \quad (2)$$

where Δf_{th}, Δf_{s}, Δf_{o}, and Δf_{slot} are corrections, obtained by perturbation theory,[24,27,29,32,36−38] for the thermal boundary layer at the wall, coupling of the gas and shell motion, tubular openings in the wall to admit gas, and closed-end slots around the transducer housings. For a nonthermally relaxing gas within a spherical cavity two of these interactions occur at the interface between the gas and the shell and determine the range of densities over which precise sound-speed measurements can be obtained from radial modes.

The first of these is the thermal boundary layer Δf_{th} that exists at the cavity walls as a consequence of the nonzero thermal conductivity of the gas and the boundary conditions that constrain the temperature and velocity fields at that surface.[23,29,36] The thermal boundary layer gives rise to a fractional shift in the resonance frequencies, relative to an idealized case in which heat transfer is ignored at the wall, that varies according to $(f\rho)^{-1/2}$ and becomes important at low frequencies f and low densities ρ; at pressure below about 1 MPa and certainly at pressure below 0.1 MPa, the thermal boundary layer dominates the corrections that must be applied to the experimental resonance frequencies. In this work, the thermal boundary layer was determined from the expression described by Ewing et al.[36] with a thermal accommodation coefficient of unity.

The second interaction occurs between the gas and the wall in which the wall responds elastically to the acoustic pressure acting there. The resulting wall motion is microscopic but gives rise to a shift in the resonance frequencies Δf_{s} relative to a cavity with rigid walls. The wall motion varies in proportion to ρu^2 at frequencies far from a resonance of the cavity wall and hence is of growing importance as the gas pressure is increased.[27,37] The effect also increases as the frequency of the gas resonance tends toward that of the shell to the extent that useful measurements cannot be made at any density.[37,38] A generalized theory for the motion of a thick spherical shell to include both radial and nonradial acoustic modes has been reported.[37] Although direct coupling between the gas and the shell motions is dominated by overlap of modes with the same symmetry, evidence has been reported of nonradial shell motion coupling to the radial modes in the gas,[38−40] based on the relative uncertainty in sound speed determined from $(0, n)$, $n = 2, 3, 4, 5, ..., \gg 10^{-5}u$. Moldover et al.[27] have considered the additional effect of radiative losses from the external surface of the shell for pressure compensated resonators that is a potentially important loss mechanism not encountered in this work.

A spherical resonator is usually constructed from two hemispheres joined at the equator and often has transducers which are inserted into the wall as removable units. Both of these mechanical arrangements leave annular slits between the two hemispheres or the transducer housing and the wall. Trusler et al.[38,41] have determined the effect of Δf_{slot} on the radial resonance frequency and half width in a spherical cavity for a slit bounded by semi-infinite parallel flat surfaces. For a 10 mm deep slot 10 μm wide around a transducer of 12 mm diameter located in the 45 mm radius resonator, the correction to the frequency is fractionally less than $3 \cdot 10^{-6}$ and the contribution to g/f less than $5 \cdot 10^{-6}$.

The perturbation Δf_{o} arising from an open tube[39] is proportional to $\cot(\nu_{0,n}L/a)$ and the eigenvalues $\nu_{0,n}$ of the $(0, n)$ radial modes are approximately $(n - 1/2)\pi$ where $n = 2, 3, ...$, so that when $L \approx a$ there is a fractional perturbation to the radial resonance frequencies on the order of 10^{-6}.

When the resonator was filled with argon, the results obtained from eq 1 have been used to determine the resonator's radius $a(T, p = 0)$ and second β_{a} acoustic virial coefficient by analysis in terms of the expansion:

$$[u/a(T,p=0)]^2 = [A_0/a(T,p=0)^2][1 + \{\beta_{\mathrm{a}}(T)/RT\}p + \{\gamma'_{\mathrm{a}}(T)/RT\}p^2 + ...] \quad (3)$$

where

$$A_0 = \frac{RT\gamma^{\mathrm{pg}}}{M} \quad (4)$$

and

$$a(T,p=0) = \{(RT\gamma^{\mathrm{pg}}/M)[a(T,p=0)^2/A_0]\}^{1/2} \quad (5)$$

In eq 4, R is the gas constant, $\gamma^{\mathrm{pg}} = C_{p,\mathrm{m}}^{\mathrm{pg}}/(C_{p,\mathrm{m}}^{\mathrm{pg}} - R)$, $C_{p,\mathrm{m}}^{\mathrm{pg}}$, the isobaric perfect-gas molar heat capacity, and M the molar mass. In eq 5 the term $[a(T, p = 0)^2/A_0]$ is an adjustable parameter obtained by regression analysis. The calibration procedure to determine a is possible because both $C_{p,\mathrm{m}}^{\mathrm{pg}}$ and M are known with sufficient certainty for a monatomic gas.[22]

For gases at low and moderate densities, eq 3, for $p(T, \rho_n)$, and

$$\{u/a(T,p=0)\}^2 = A_0[1 + \{\beta_a(T)/RT\}\rho_n + \{\gamma'_a(T)/RT\}\rho_n^2 + ...]/a^2(T,p=0) \quad (6)$$

for $u^2(T, \rho_n)$, both converge rapidly. Typically, only the leading three or four terms of eqs 3 and 6 are required to reduce the truncation error to the order of usual experimental error.[10,42−44] Equation 3, for $u^2(T, p)$, converges rapidly,[24,35] but there is empirical evidence that, compared with eq 6, convergence is less rapid at subcritical temperatures.[43] For measurements at temperatures above critical, and over a wide pressure range, more terms may be required to represent the results for the whole isotherm.

Equation 3 shows that the determination of $u(T, p)$ requires $a(T, p)$, while obtaining $C_{p,m}^{pg}(T)$ requires solely $a(T, p = 0)$, and obtaining acoustic virial coefficients requires knowledge of the ratio $a(T, p)/a(T, p = 0)$. The $a(T, p)$ were obtained from $a(T, p = 0)$ combined with the compliance of the resonator $a^{-1}\cdot(\partial a/\partial p)_T$, that were, in this case, estimated under conditions of constant external pressure equal to the local atmospheric pressure of about 90 kPa, from literature values for the elastic constants to give the ratio $a(T, p)/a(T, p = 0)$ of eq 1; elastic constants obtained from the literature were used, and these are discussed in the Experimental Section under Data Sources. The $u(T, p)$ results are then multiplied by the factor $u(T_n)/u(T)$ to account for the difference between the actual temperature T of the measurements and the nominal temperature of the isotherm T_n. Provided that $|T_n - T|$ is less than about 0.1 K, this procedure should not introduce a significant additional uncertainty.

Apparatus and Experimental Section

The apparatus was designed to operate at pressures up to 42 MPa and at temperatures below 500 K. Each component was manufactured from type 316 stainless steel with either mechanical or electro-polished internal surfaces. The apparatus consisted of two spherical acoustic resonators, one of a 45 mm radius and the other of a 25 mm radius, a re-entrant radio frequency cavity, a concentric cylinder capacitor, and a circulating pump assembled without recourse to elastomers and housed in a thermostat to permit simultaneous determination of the physical properties on one fluid sample. This article is concerned with the spherical acoustic resonators and ancillary components. Methods of determining the complex relative to electric permittivity will be described in a subsequent publication. All measurements of resistance, temperature, pressure, mass, and frequency were directly traceable to national standards.

Spherical Resonator. Two spherical resonators were constructed for this work, one with a nominal internal radius of 45 mm, shown in Figure 1, and the other an internal radius of about 25 mm, shown in Figure 2. The spheres were similar in some respects to those described in the literature.[13,14,27,30,39,40,45,46] The procedure used to machine the nominal 45 mm radius resonator is described; a numerical controlled lathe was used to fabricate the 25 mm radius sphere with a wall thickness of 38 mm.

The spherical resonator, shown in Figure 1, was constructed as two hemispheres from a single cylindrical bar of {0.6585Fe + 0.0008C + 0.02Mn + 0.00045P + 0.0003S + 0.01Si + 0.17Cr + 0.12Ni + 0.02Mo} commonly known as 316L austenitic stainless steel to form a cavity with a nominal internal radius of 45 mm. Before turning commenced, the two-transducer ports were drilled along with two openings that allowed fluid to flow into and out of the cavity. The transducer ports were drilled at a polar angle of $\pi/4$, separated by an azimuthal angle of π in the upper hemisphere, and then reamed to a diameter of 12.7 mm. This geometric arrangement reduced the efficiency with which the symmetry forbidden (3, 1) resonance is detected in comparison with the radially symmetric (0, 2) resonance even for transducers with nonzero surface area in an imperfect sphere. These ports were then plugged, and the interior surface of each hemisphere was turned with a worm-driven tool. The external surface was formed into cones, to give a wall thickness of about 42 mm, and the surfaces located next to the transducer ports were ground until they were perpendicular to the housing receptacle. Tooling marks on the interior surface were reduced by mechanical polishing, and any resulting rounding of the equatorial edge was subsequently removed in the final dimensional adjustment. The polishing was effected with Jewelers rouge and aluminum oxide powder of average diameter of 1 μm suspended in cutting oil. The hemispheres were then machined at the equator to form an interlocking step B, which ensured accurate concentric alignment about the polar axis. A groove suitable for a silver O-ring A was machined into the equatorial surface. The step made metal-to-metal contact from the outer edge of the O-ring groove to the inner spherical surface but not where the bolts passed through both hemispheres. To

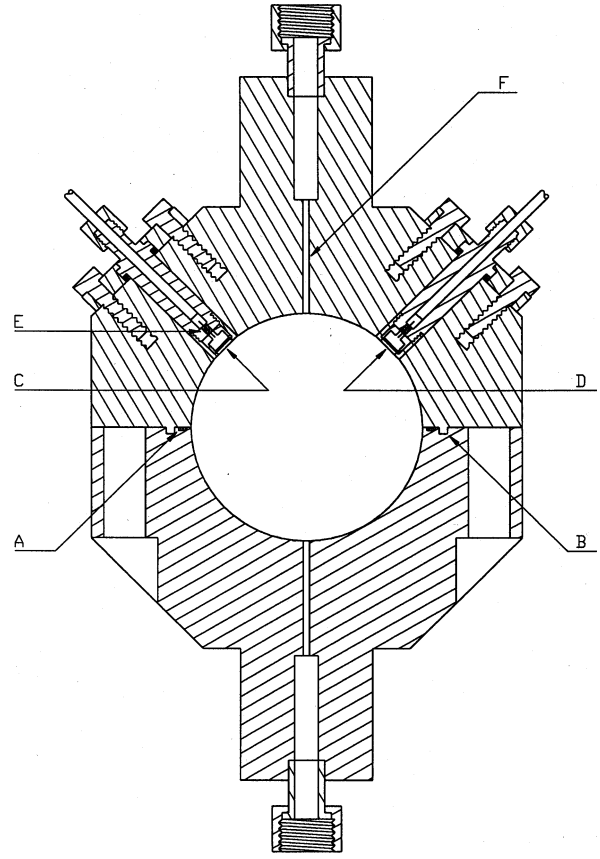

Figure 1. Cross-section through a spherical resonator fabricated as two hemispheres from a single cylindrical bar of type 316L stainless steel to form a cavity with a nominal internal radius of 45 mm.[5] The acoustic transducers were fabricated to fit within ports, and each housing was sealed with a silver O-ring with separate flanges and bolts. The gas under test was sealed by a glass-to-metal seal E so that it was exposed to the transducer back-plate and active diaphragms C and D that were mounted flush with the resonator's interior surface. The hemispheres were then machined at the equator to form an interlocking step B, which ensured accurate concentric alignment about the polar axis, and made metal-to-metal contact at the inner spherical surface. A groove suitable for a silver O-ring A was machined into the equatorial surface. To form the 2.4 mm diameter inlet tubes for fluid flow in each pole, a hole was drilled to a total of 45.7 mm F, and the remaining 48 mm of the boss was opened out to a radius of 9 mm. A face-seal fitting was welded into the outer end of the larger diameter tube.

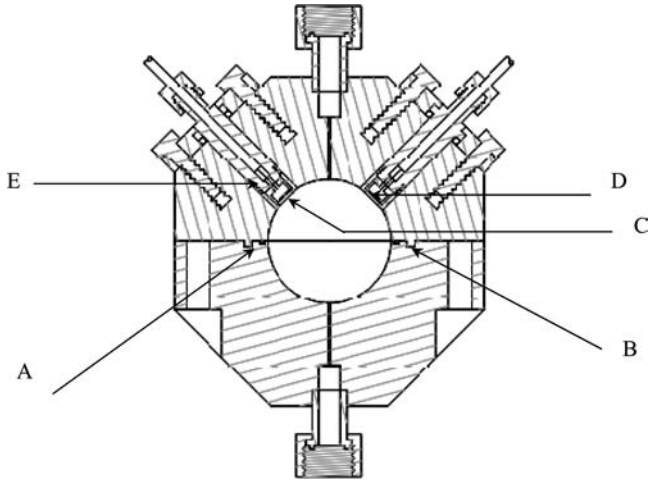

Figure 2. Cross-section through a spherical resonator fabricated as two hemispheres from a single cylindrical bar of type 316L stainless steel to form a cavity with a nominal internal radius of 25 mm.[5] The acoustic transducers were fabricated to fit within ports, and each housing was sealed with a silver O-ring with separate flanges and bolts. The gas under test was sealed by a glass-to-metal seal E so that it was exposed to the transducer back-plate and active diaphragms C and D that were mounted flush with the resonators interior surface. The hemispheres were then machined at the equator to form an interlocking step B, which ensured accurate concentric alignment about the polar axis, and made metal-to-metal contact at the inner spherical surface. A groove suitable for a silver O-ring A was machined into the equatorial surface. To form the 1.02 mm diameter inlet tubes for fluid flow in each pole, a hole was drilled to a total of 25.4 mm, and the remaining opened to a radius of about 9 mm. A face-seal fitting was welded into the outer end of the larger diameter tube.

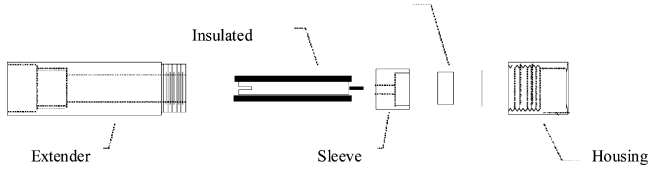

Figure 3. Cross-section through the electro-acoustic transducer parts separated for the sake of clarity.

form the 2.4 mm diameter inlet and outlet tubes F for fluid flow in each pole, a hole was drilled to a total of 45.7 mm from the inner spherical surface, and the remaining 48 mm of the boss was opened out to a radius of 9 mm. A face-seal fitting, with a metal gasket, was welded into the outer end of the larger diameter tube.

Transducers. Solid dielectric capacitive transducers, which form part of the wall of a resonator, were used for this work as described in refs 9, 29, 47, and 48. They consisted of a rigid back-plate separated from a metallic diaphragm by a gas-filled gap. For the transducers shown in Figures 1, 2, and 3 the dielectric layer was formed by melting glass powder on the back-plate[6,9] and combined with a metal film to create a capacitor; pressure equalization was achieved by a hole in the metal foil. The whole transducer consisted of a cylindrical extension, a cap, a Kovar plate, a ceramic insulating sleeve, and a backing flange; Kovar is by mass fraction {0.54Fe + 0.29Ni + 0.17Co + < 0.0001C + 0.002Si + 0.003Mn} and gives a linear thermal expansion compatible with borosilicate glass. The Kovar plate was one of the elements of the capacitor and was electrically isolated from the transducer body by the ceramic sleeve. The active element of the capacitive transducer was formed from a 9.5 mm diameter disk of 6 μm thick aluminum foil which was electrically connected to the body of the transducer. The Kovar back-plate and ceramic sleeve were sprayed with Corning powdered glass and suspended in acetone, and the glass was melted in a furnace purged with either argon or nitrogen at a temperature of about 800 K; the furnace temperature was increased at a rate between (0.1 and 0.3) $K \cdot s^{-1}$. The furnace was then maintained at $T = 811$ K for about 180 s before cooling to $T = 293$ K. An electrical feedthrough was assembled in the cylindrical extension from a glass bead and Kovar wire fused to the metal flange by heating to a temperature of about 922 K. The diameter of the cylindrical extension was adjusted to create a sliding fit within the resonator port with a nominal clearance of 10 μm to reduce the area of the annular slot. The length of the cylindrical extension was adjusted to ensure the inner surface of the transducer, and the resonator was flush when fitted with the cap and glass-coated Kovar. The cap, which held the foil and glass-coated electrode, was threaded onto the cylindrical extension and the surface that formed part of the internal wall of the resonator machined to match the radius of curvature of the sphere. When the transducer was assembled with a 6 μm thick aluminum foil disk, the capacitance was between (10 and 30) pF without an applied direct current (dc) bias. The transducers were tested with a dc bias of up to 350 V without failure, and they maintained satisfactory electrical characteristics when tested to temperatures up to 700 K. The rectangular flange located on the outer surface of the resonator was used to retain the transducers and was constructed from heat-treated steel.

Electrical connections were made to the source with a coaxial cable, while the triaxial cable was used for the detector. The central conductor of these cables was connected to a pin that fitted a receptacle crimped to the outer part of the Kovar wire inside the cylindrical extension of the transducer body. The shield was connected to the resonator with the Swagelock retaining nut; only the inner shield of the microphone triaxial cable is connected to the ground with the outer shield permitted to float.

Circulating Pump. Two circulating pumps were used for this work, and both were adapted from designs reported in the literature.[49−52] The first was similar to that reported by Goodwin et al.[16,17] and Kandil et al.;[18,19] neither were as sophisticated as that reported by Peleties et al.[53] The second, shown in Figure 4, was constructed from 316L austenitic stainless steel to withstand an internal pressure of 69 MPa. The internal diameter was honed to 6 mm over a length of about 142 mm. Prior to final honing, a number 6 VCR gland was welded to one end and a block to the other. The upper gland was threaded to accept a restraint which prevented the piston from exiting the cylinder during operation. The piston was machined from {0.8478Fe + 0.0015C + 0.01Mn + 0.0004P + 0.0003S + 0.01Si + 0.13Cr} commonly known as type 420 martensitic stainless steel. The piston was 50 mm long and had a 3.2 mm diameter hole drilled along the cylindrical axis, and perpendicular to it at a length of 5.8 mm from one end a rectangular hole was bored; the piston had no threaded parts as was the case in previous designs.[16−19] Prior to inserting the piston within the cylinder, a sapphire sphere was placed into the rectangular hole to serve as a check-valve. The piston was moved within the cylinder by an external electromagnet which was formed from about 300 turns of glass-coated wire wound directly to the outer surface of the cylinder. The assembled pump was installed within the apparatus so that the bottom of the piston stroke was located at the lowest plane in the fluid handling system.

The pump was activated at a frequency of about 1 Hz with 110 V alternating current (ac) and provided a volume displace-

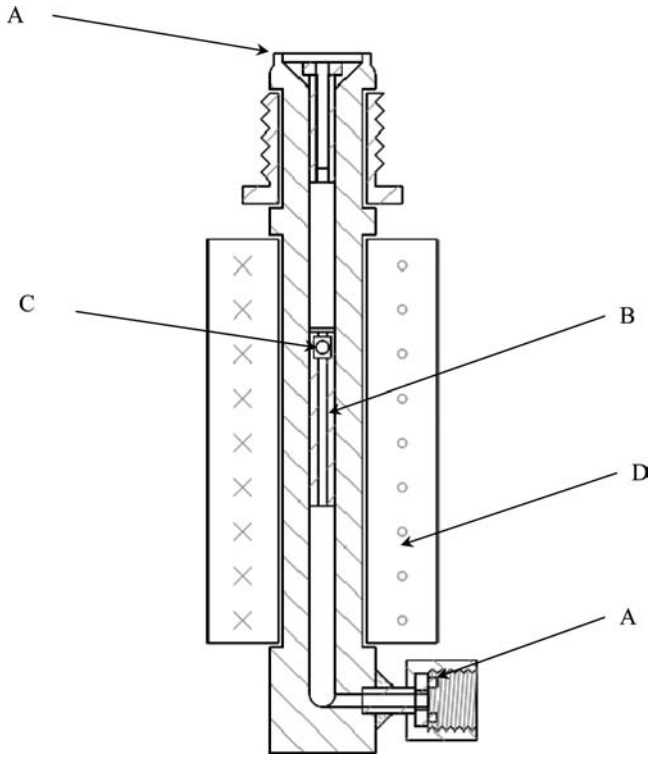

Figure 4. Cross-section through a schematic of the magnetically activated pump used to circulate the fluid through the differential pressure gauge, spherical resonators, concentric cylinder capacitor, re-entrant cavity, and interconnecting tubing. The pump A is formed from a piston B within a cylinder C. The piston B was fabricated from type 420 martensitic (magnetic stainless steel) and is fitted with a check-valve C formed from a sapphire sphere within a cavity that promotes flow in the upward direction. The piston was forced to move by a electromagnet D mounted outside the cylinder that was fabricated from type 316 austenitic stainless steel.

ment of about 0.3 $cm^3 \cdot s^{-1}$ when tested with water at ambient temperature and pressure.

Frequency Measurement. The sinusoidal source was generated by a frequency synthesizer (SRS DS345) that was phase-locked to a LOng Range Aid to Navigation (LORAN) version C at 10 MHz with an fractional uncertainty of 10^{-10}. LORAN-C is a terrestrial radio navigation system operated at frequencies between (90 and 110) kHz by the U.S. Coast Guard.[54] The signal, with a maximum output of 10 V p-p, was connected to a universal counter, reference channel of a digital lock-in amplifier, and a switch and control box (HP 3488A fitted with a 44472A card). The latter determined which spherical resonator received the signal after amplification by a power amplifier (Krohn-Hite 13724A set with about 6 dB gain) to give a signal of about 150 V root mean square (rms); the source is operated as a square law device, and signal clipping can be tolerated. The counter independently monitored the frequency output by the synthesizer. An additional advantage of capacitive transducers is that, when excited by a signal from a frequency synthesizer without a dc bias, sound is produced at a frequency twice that of the feed and renders negligible electrical cross-talk between the transmitter and the receiver.

The detector transducer has an active capacitance of $\approx$ 30 pF and therefore acts as a very high impedance signal source when the membrane is set in motion by audio frequency sound. It was connected by an about 0.5 m long Teflon insulated triaxial cable of capacitance of $\approx$15 pF to a junction field-effect transistor (JFET) of unity gain[29,55,56] that effectively matched the high impedance of the microphone preventing the division of the signal by the ratio of stray-to-active capacitance and permitted a coaxial cable of length > 2 m to connect with the instrumentation. This JFET preamplifier housing also contained connections for 200 V dc bias, found by observation to provide the optimal signal-to-noise ratio. The preamplifier output was connected to a band-pass filter (Stanford Research Systems, CA, model SR560) set to pass frequencies between 300 Hz and 100 kHz with a gain of 10 and then to another channel of the switch and control and ultimately a lock-in amplifier operated in frequency doubling (2*f*) mode.

The source transducer was excited at frequencies *f* from ($f_{0,n}$ $-$ $g_{0,n}$) in steps of $g_{0,n}/5$ to about ($f_{0,n} + g_{0,n}$) where *g* is half of the resonance line width at $2^{-1/2}$ the maximum amplitude. At each frequency the in-phase and quadrature voltage of the received voltage are compared to that sent with a lock-in amplifier and then fit to obtain the complex resonance frequency[57,58] with an uncertainty of about $10^{-6}f$.

Pressure Measurement and Control. The fluid under test was separated from the pressure gauges and controllers by a differential pressure transducer (DPT) which was operated as a null instrument. This separator was located within the thermostat atop the circulation pump that was fitted with a tube to promote circulation through the cavity of the DPT containing the diaphragm. There were two pressure controllers, each containing a resonant quartz pressure transducer, that were used to automatically maintain the DPT close to the null, and a digital piston gauge. These three pressure gauges were operated relative to atmospheric pressure that was determined with a quartz barometer. The precision of each instrument will be described.

The DPT (Sensotec model HL-Z/9424−01) had a span of 0.34 MPa at line pressures up to 69 MPa, and the membrane stress was determined with a strain gauge that was excited by 10 V dc. The supplier of the DPT cited a precision in pressure of 0.5 kPa. The null of the DPT was determined at 10 line pressures up to 10 MPa and found to vary by no more than about −4.5 kPa with a hysteresis and linearity of about 0.2 kPa. These results are within the manufacturer's cited specifications and introduce a ($k = 1$) uncertainty in pressures of no more than 200 Pa. The DPT span was calibrated but is considerably less critical to the precision of the pressure measurements because in this application it was used as a null instrument.

The two pressure controllers supplied by DH Instruments (DH) were a DH PPC2, which was used for pressures below 7 MPa, and a DH PPCK-P6 that operated at pressures up to 42 MPa. Each controller was equipped with a quartz pressure gauge with an uncertainty, cited by the manufacturer, of 0.02 % of full scale pressure. For the PPC2 this implies an uncertainty of 1.4 kPa, while the gauge installed within the PPCK-P6 was calibrated for operation at three discrete pressure ranges and had uncertainties determined by the following upper limits: (1) 14 MPa where $\delta p \approx 2.8$ kPa, (2) 28 MPa where $\delta p \approx 5.6$ kPa, and (3) 42 MPa where $\delta p \approx 8.4$ kPa. Both the PPC2 and the PPCK-P6 controlled the pressure of the reference gas, which was dry-oil free nitrogen with a mole fraction purity of 0.99998, by continually leaking fluid to the atmosphere.

To measure and control pressures below 110 kPa, the PPC2 reference port was connected to a rotary vacuum pump which was able to provide a pumping rate of about 50 $m^3 \cdot h^{-1}$, sufficient to overcome the PPC2 leak rate while maintaining the reference pressure below the minimum desired control pressure.

A DH digital piston gauge (DPG, balance 26000) operated at pressures up to 50 MPa could be connected to the reference port of the DPT or either pressure controller. The DPG had an

uncertainty, cited by the manufacturer, of (2.5 kPa + 0.0001p), where p is the measured pressure, and had an uncertainty less than that provided by the PPCK-P6 at pressures greater than 28 MPa.

Atmospheric pressure was determined with a Paroscientific quartz barometer (model 740-16B) with a resolution of 0.1 Pa and an uncertainty, cited by the manufacturer, of about 10 Pa.

Small hydrostatic head corrections have been applied to the quoted pressures so that the values refer to a distance ≈ 0.05 m below the diaphragm of the DPT and equivalent to the equator of the 45 mm sphere. Three separate head corrections were applied: (1) for the density of a 0.05 m height of sample, (2) for the 0.27 m of nitrogen in the thermostat, and (3) for the height of nitrogen, at atmospheric temperature, between the top of the thermostat and the pressure gauge utilized for the measurement. The nitrogen head corrections for the PPC2, PPCK-P6, and DPG were, in the worst case, 300 Pa, 110 Pa, and 1.4 kPa, respectively. A head correction of < 8 Pa was applied to the cited pressure to account for the height difference between the DH gauges and the barometer. All of these head corrections are at least a factor of 2 less than the uncertainty arising from the pressure gauge itself. The density required in these calculations was determined from the National Institute of Standards and Technology, Standard Reference Database 23 Version 7.1, commonly known by the acronym REFPROP.[59]

The worst case fractional uncertainty in the speed of sound arising from the imprecision in pressure p can be estimated for each pressure gauge from $u^{-1}(\partial u/\partial p)_T$. For argon at $T = 310$ K and $p = 5.8$ MPa, the worst case for these measurements, is $u^{-1}(\partial u/\partial p)_T = 5 \cdot 10^{-3}$ MPa^{-1},[60] and the uncertainty in sound speed is $< \pm 7 \cdot 10^{-6} \cdot u$ for the PPC2, $< \pm n \cdot 10^{-5} \cdot u$, where the range number $n = 1$, 2, or 3, for the PPCK-P6, and $\pm 4 \cdot 10^{-5} \cdot u$ for the DPG at $p = 50$ MPa.

Temperature Measurement. The temperature of the fluid under testing was determined with a Rosemount capsule platinum resistance thermometer (PRT) (type 162D, serial number 4050) inserted within a well in the center of the radio frequency re-entrant cavity.[15,16,18] This blind hole passes down inside the bulbous extension of the top plate and was thermally connected to the re-entrant cavity with Swagelock Silver Goop. This PRT had a nominal resistance at a room temperature of 25 Ω and was calibrated on ITS-90. The speed of sound u varies in proportion to $T^{1/2}$, where T is the thermodynamic temperature, and at $T = 300$ K, where the fractional uncertainty in ITS-90 is about $3 \cdot 10^{-6}$;[61,62] the uncertainty in the speed of sound arising from uncertainties in temperature is $\pm 2 \cdot 10^{-6} \cdot u$. The resistance of the four-wire PRT was determined with an Automatic Systems Laboratory model F17A ratio comparator bridge operated at a frequency of about 375 Hz and a current of 1 mA. The bridge determined the ratio of the resistance of the PRT to that of a standard resistor with a resolution that corresponds to an uncertainty in temperature of about 1 mK for ratios < 4. The external standard for this PRT was a Wilkins type resistor (serial number 267923) manufactured by Tinsley that has been calibrated at a temperature of 293 K, a current of 30 mA, and a frequency of 400 Hz and found to have a resistance of $(24.9999_8 \pm 0.0001_0)$ Ω and $dR/dT = 0.25 \cdot 10^{-6}$ Ω·K^{-1} at temperatures between (291 and 303) K. The temperature of the Wilkins resistor was determined with a 100 Ω PRT, located in a copper block in the center of the resistor, with a precision better than 0.1 K. The temperature was determined from the measured resistance on ITS-90.

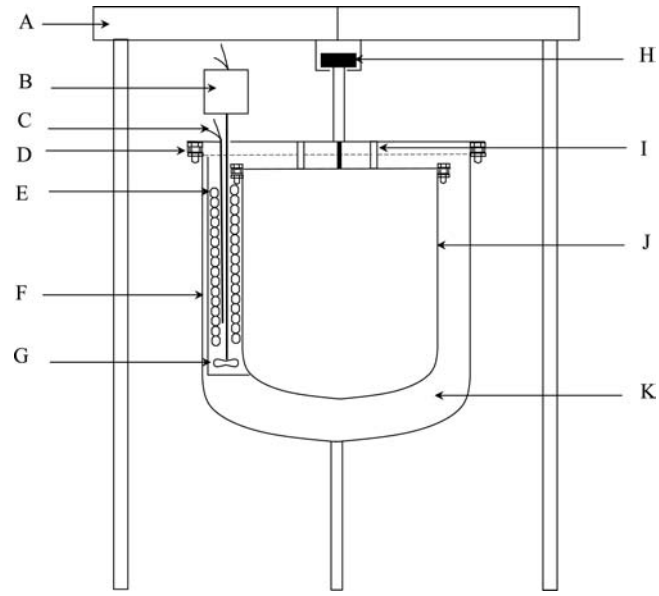

Figure 5. Schematic of the apparatus showing the support frame A, stirrer motor B, 1 kW heater C, flat-ring seal D, cooling coil E, stirrer baffle F, stirrer propeller (one of two shown) G, rubber isolated mount H, interconnecting tubulars for the passage of wires to apparatus I, inner can separating the apparatus from the stirred fluid contained between J and the outer canister, and stirred fluid K with the level maintained at about the dashed horizontal line.

The temperature of the stirred fluid thermostat bath fluid was determined with a 100 Ω ASL metal-cased thermometer independently calibrated on ITS-90 with an uncertainty of ± 0.01 K.

A long-stem glass-sheathed PRT (YSI type 8163QB, serial number 4721) with a nominal resistance of 25 Ω, also calibrated on ITS-90, was used as the laboratory comparison standard against which industrial grade 100 Ω thermometers were calibrated, including those located to determine temperatures of (1) the Wilkins standard resistor and (2) the DH Instruments pressure controllers and DPG and (3) to estimate the contribution to pressure of the hydrostatic head. The temperature indicated by these thermometers had an uncertainty of ±0.1 K. These thermometers were connected to the ASL bridge through a switch box (HP 3488A S/N 2719A-30591) fitted with two HP44471a cards to determine the resistance ratio relative to the ASL internal nominal 100 Ω resistor.

The temperatures of the chilled circulator reservoir and of seven locations on the gas handling system, including valves, the supply cylinder, and interconnecting tubing, were determined with thermocouples using a Stanford Research Systems thermocouple monitor SR 630 S/N 17602 with an uncertainty of about ±1 K.

Thermostat and Temperature Control. The thermostat, shown schematically in Figure 5, was assembled from two canisters formed from galvanized cylinders, each closed at one end with a dome and a flange on the opposite end to form containers that fit one inside the other,[5] a bar, two circular plates to which the beakers were bolted, and a coupler from which the complete assembly hung on a three-legged stand. In this arrangement the cylindrical cans were each bolted to a circular plate, one forming the top of the beaker container, the apparatus, and the other to the outer container. Through the upper larger diameter circular plate, the gas and thermostat fluid to the lower small diameter plate were welded four 19 mm inner diameter tubes that provided the access for cables to the apparatus without immersion in the thermostat fluid. When all of the cables had

been installed, these tubes were packed with glass wool and sealed with a silicon sealer (GE Inc., RTV). The inner cylinder was bolted onto the smaller circular plate with a flat silicon ring gasket to form a fluid tight vessel. This container housed the apparatus that consisted of the spherical resonators, re-entrant cavity, concentric cylinder capacitor, electromagnetic circulating pump, and DPT that were all bolted separately onto the central vertical bar. This canister also housed cables that could withstand an operation at temperatures up to 550 K, a heating tape, a valve, and interconnecting tubing. A square sectioned tube was welded onto the outside of the inner canister. This tube acted as a baffle which extended the whole length of the can and contained the stirrer rod. On the lower 50 mm of the rod two propellers were attached to draw the bath fluid through the baffle, while the upper end of the rod was attached to a motor turning at about 1800 rpm. The baffle contained the 1 kW heater attached to a programmable power supply and also contained a cooling coil formed from about 3 m of a 6.4 mm outer diameter copper tube through which methanol was circulated from a reservoir of a refrigerator (Neslab ULT-80) that was operated at temperatures between (193 and 303) K.

The fluid flow between the thermostat and the refrigerator reservoir was started and stopped by an air-actuated ball valve that was open when the apparatus thermostat was controlled at temperatures < 313 K. For thermostat control temperatures between (273 and 313) K the refrigerator reservoir temperature was between (263 and 303) K, while for thermostat $T < 273$ K the refrigerator reservoir temperature was, according to an empirically derived relationship, determined with the requirement of optimal temperature control over the volume of thermostatted bath fluid.

The volume between the two canisters was filled with thermostat fluid and the level within the annular gap maintained between (25 and 50) mm below the top plate as determined by a pipet inserted through the orifice occupied by the bath thermometer. For operation at temperatures between (230 and 370) K the thermostat fluid was $\{0.28\ C_2H_4(OH)_2 + 0.72\ H_2O\}$, while for $T < 230$ K methanol was selected and silicon oil for $T > 370$ K.

The temperature of the thermostat was controlled by a Quantum Design (QD) digital bridge with thermistors for which $dR/dT \approx -100\ \Omega \cdot K^{-1}$ to provide temperature variations, as determined by the YSI long-stem thermometer, of ±3 mK. The output of the QD was used to drive a Sorenson (model DCS 150-7) programmable power supply capable of delivering voltages up to 150 V dc at currents up to 7 A that was connected to a 1,000 W heater, located in the thermostat baffle. To permit thermostat operation over the temperature range of (190 to 550) K four thermistors (supplied by YSI Inc. in stainless steel sheaths) were required of nominal resistances at $T = 293$ K of 300 Ω, 2 kΩ, 6 kΩ, and 10 kΩ. These were located about the midpoint of the bath-fluid depth. The $R(T)$ of each thermistor was determined by a calibration against the ASL industrial PRT at about 10 temperatures in the thermostat operating range. The $R(T)$ so determined was represented by the Steinhart−Hart formula.

The two spherical resonators, re-entrant cavity, concentric cylinder capacitor, mixing pump, and DPT have a mass greater than 100 kg and are separated from the stirred fluid by a metal wall. The volume between these components and the metal wall was filled with gas at atmospheric pressure. For these reasons the temperature of the apparatus as indicated by the thermometer within the re-entrant cavity was controlled to about ±1 mK. However, this control was in part achieved because the system had a long thermal response time constant. For example, when the bath fluid was set at a temperature 10 K above the apparatus temperature, the apparatus temperature responded at a rate of about 1 $h \cdot K^{-1}$. Two modifications were implemented to decrease the response time. First, radiation fins were installed on the apparatus components, for example, attached to both of the upper and lower bosses of the spherical resonators. Second, helium, with a thermal conductivity about six times greater than air at temperatures between (273 and 373) K and $p = 0.1$ MPa, was used to fill the inner canister. These modifications decreased the response time by about 25 %.

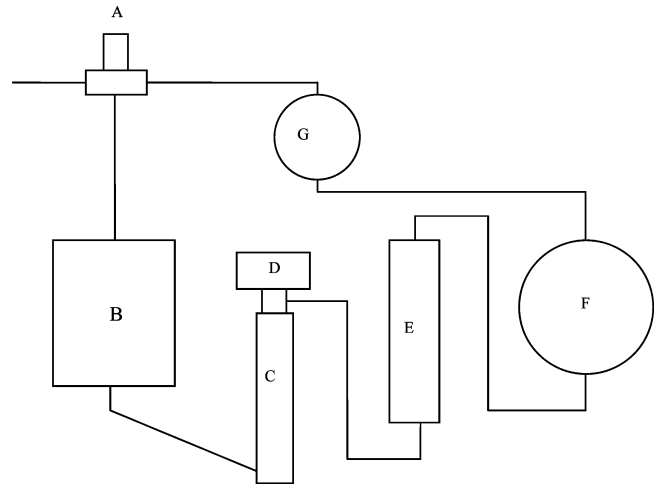

Figure 6. Schematic of the apparatus enclosed within a stirred fluid bath that includes an air-actuated bellows valve A, re-entrant cavity B, circulating pump C, DPTs D, concentric cylinder capacitor E, spherical resonator of the 45 mm internal radius F, and spherical resonator of the 25 mm internal radius G. The interconnecting lines represent the about 6 mm outer diameter tube with electro-polished internal surfaces. At the junction between the component and the tube was a Cajon VCR face-seal fitting.

Fluid Connections and Valves. The apparatus components (consisting of a valve, two spherical resonators, a re-entrant cavity, a concentric cylinder capacitor, a electromagnetic mixing pump, and a DPT) were interconnected, as described below, with electropolished stainless steel 1/8 in. outer diameter tubing, except for a part required to transition to the DPT. To facilitate remixing, crevices and "dead" volumes were kept to a minimum to reduce trapping droplets and bubbles. To prevent fluid condensation in the filling lines, all of the external tubes were trace heated. The trace heating also assisted in the removal of water during evacuation. Fluid flows into the apparatus, shown in Figure 6, through a normally closed air actuated valve (Nupro HB series) that is located in the thermostat to eliminate the possibility of fluid condensing in the tube between the apparatus and the external gas handling system. This straight-through valve has been modified by the addition of metallic face-seal fitting (number 2 Cajon VCR) welded into the base of the body and in this arrangement permits fluid to be circulated through the valve while closed to significantly reduce the dead volume. The fitting within the valve base was connected atop the re-entrant cavity, while the valve inlet connected to the gas handling system and the original outlet to atop the nominal 25 mm radius sphere. The fluid outlet in the base of the re-entrant cavity was connected to the lower end of the circulating pump, which was the lowest point in the whole apparatus. The upper outlet of this pump when operating forced fluid to flow into the DPT that reduced the possibility of trapping fluid in the dead volume formed by the DPT. After leaving the DPT, fluid flows into the top of the concentric cylinder capacitor where it flowed between

the two cylinders that form the capacitance. The fluid exited the base of the concentric cylinder capacitor and entered the bottom of the 45 mm radius spherical resonator. The top of this resonator was connected to the base of the 25 mm sphere.

Seals. Gas tight seals between the tubes and the apparatus components were formed with Cajon VCR glands and gaskets, while those between the fabricated metal parts were formed with either solid metallic O-rings or gas-filled metal O-rings that were preferred owing to chemical compatibility. For metallic O-rings, the sealing surfaces were machined to a surface finish of less than 16 μm rms with remaining machining marks forming concentric circles within the groove. The solid O-rings were formed from either aluminum, silver, or gold with silver being the preferred material. Not surprisingly, rings made from aluminum were the least reliable at maintaining a seal between stainless steel parts after temperature and pressure cycling. Gold O-rings, used to seal the transducer ports, were also fabricated in our laboratory with the material and procedures described below.

Gold wire of a cross-sectional diameter 1.016 mm (or 0.040 in.) was used to fabricate O-rings with the following procedure: (1) gold wire was wrapped about a tapered mandrel, specifically fabricated for the purpose, and cut roughly to the required length for the groove with a razor blade; (2) the wire ends were cut to be perpendicular to the cylindrical surface; (3) wire was formed in a loop, and the ends were butted together; (4) a blue-colored flame was formed from the combustion of (butane + N_2O) and used to fuse the wire-loop to an O-ring by melting; (5) the wire ring was annealed with the (butane + N_2O) flame; (6) the O-ring stretched over the circular mandrel to form a ring of correct diameter; (7) the O-ring annealed prior to use.

Vacuum Pumps. The apparatus was evacuated though the gas handling system with a Leybold turbo-molecular pumping station. This consisted of a turbo-molecular pump and a direct drive rotary vacuum pump. The gas handling system was connected to an approximately 20 mm outer diameter vacuum cross with a 6.35 mm VCR connector. At this cross-junction were also located a manual valve, a vacuum gauge, and a transition to an about 40 mm outer diameter bellows vacuum tubing. The manual valve allowed the vacuum system to be used separately from the apparatus. The 40 mm bellows tube was connected to a trap, which was connected to the turbo-molecular pump with a right angle fitting. The pressure within the vacuum system was determined, dependent on the pressure, with either an ionization or thermal conductivity gauge. The pressure measured immediately before connection to the gas handling system was less than $< 10^{-4}$ Pa, and the apparatus was connected to this through an about 1 m long 0.8 mm inner diameter tube.

Materials. The argon was supplied by Matheson as ultra high purity with a mole fraction of $x > 0.99999$ and was used without further purification. The supplied cited from gas chromatography the following mole fraction impurities: total hydrocarbon $x < 0.5 \cdot 10^{-6}$, $x(O_2) < 1 \cdot 10^{-6}$, $x(CO_2) < 1 \cdot 10^{-6}$, $x(H_2O) < 1 \cdot 10^{-6}$, $x(N_2) < 4 \cdot 10^{-6}$, and $x(H_2) < 4 \cdot 10^{-6}$. In this work we assume the molar mass of argon[63] $M(\mathrm{Ar}) = 0.039948\ \mathrm{kg \cdot mol^{-1}}$ and the perfect gas heat capacity $C_{p,\mathrm{m}}^{\mathrm{pg}} = 5R/2$ where $R = 8.314472\ \mathrm{J \cdot K^{-1} \cdot mol^{-1}}$.[64]

Data Sources. The density, viscosity, and thermal conductivity of argon, required in the calculation of the perturbations, were obtained from the equation of state reported by Tegeler et al.[60] and the transport property correlation of Lemmon and Jacobsen;[65] both literature sources were coded within ref 59. The uncertainty in the estimated density is $< \pm 0.02$ % and about $\pm$ 2 % for both viscosity and thermal conductivity.

The speed of sound in stainless steel, required for the shell correction, was calculated from values of Young's modulus and Poisson's ratio reported by Ledbetter.[66] The values of Young's modulus from ref 66 were fitted to a theoretical expression proposed by Varshni[67] and used by Ledbetter.[68] Poisson's ratio was represented by a polynomial in temperature. These elastic constants were used to determine $a(T, p)$ from measurements of $a(T, p = 0)$ under conditions of constant external pressure. The linear thermal expansion coefficient was obtained from ref 69 and the temperature dependence of the thermal expansion coefficient represented by an expression of the functional form advocated by Kroeger and Swenson.[70] The density of the stainless steel was determined from the mass of a billet, remaining from machining process, of known dimensions at $T = 298$ K combined with the linear thermal expansion coefficient. The thermal accommodation coefficient was taken as unity. These data sources provided properties with sufficient certainty to estimate the acoustic perturbations without introduction of significant systematic errors assuming the acoustic model represented the experiment described.

Results and Discussion

All of the selected modes were initially used in the regression to eq 3 to determine $a(T, p = 0)$ and β_a rather than just $\langle u/a \rangle$ at each pressure on an isotherm. At pressures below 0.3 MPa the (u/a) obtained from radial modes (0, n), with $n = 2$, 3, 4, 5, and 6, spanned $10^{-5}u$ and confirmed that corrections to the frequency for openings, slots, and the thermal boundary layer were applied adequately. At a pressure of about 1 MPa the thermal boundary correction, which varies in proportion to p^{-1}, is equivalent in magnitude to that arising from shell motion for a stainless steel envelope of the 45 mm internal radius. At $p >$ 1 MPa the shell motion dominates corrections to the resonance frequency that are determined from elastic theory for a thick walled isotropic spherical shell; resonators are neither spherical nor isotropic when machined and fitted with acoustic transducers. The variation with respect to the temperature of the sound speed in a gas is greater than of the elastic constants of the sphere wall, and not surprisingly, an acoustic mode may be perturbed by shell motion at one temperature but not another. Thus, observations of the difference between (u/a) obtained from each resonance frequency from the mean $\langle u/a \rangle$ combined with the excess fractional resonance line widths at a temperature and pressure formed the basis for omitting modes from the regression analysis with eq 3; the procedure adopted is similar to that described elsewhere and elucidated here.[39,40,45,71−73] The systematic departure of (u/a) obtained with a mode from the $\langle u/a \rangle$ was interpreted in terms of coupling between gas and shell modes. For all isotherms the values of (u/a) obtained from the selected modes span $10^{-5} \cdot u$ at a temperature and pressure over the full pressure range, and this internal consistency is comparable with that obtained in other resonators.[39,40,44,71−73] The fractional excess line widths, defined by $\Delta g/f = \{g(\mathrm{expt}) - g(\mathrm{calc})\}/f$, where g(expt) is the measured line width and g(calc) values determined from the acoustic model including bulk dissipation are another means of determining otherwise unaccounted energy losses and were also considered. The following three paragraphs are a digression from the discussion regarding the resonators radii and second acoustic virial coefficients determined from the sound speed measurements to consider in further detail the modes omitted.

For the 45 mm radius resonator the difference between the (u/a) obtained from mode (0, 5) and the mean $\langle u/a \rangle$ increased

Table 1. Resonator Radius $a(T, p = 0)$, the Second Acoustic Virial Coefficient β_a, and the Relative Standard Deviation of the Fit $s(u/a)^2/\{u(p = 0)/a)\}^2$ Where $s(u/a)^2$ Is the Standard Deviation at Temperature T[a]

T	$a(T, p = 0)$	β_a	
K	mm	$cm^3 \cdot mol^{-1}$	$10^6 s/u$
	October 1995		
320.000	44.4442 ± 0.0028	15.79 ± 0.18	94
310.000	44.4382 ± 0.0013	13.91 ± 0.16	30
300.000	44.4306 ± 0.0013	12.12 ± 0.16	39
290.000	44.42407 ± 0.00072	9.533 ± 0.084	20
280.000	44.4181 ± 0.0018	7.51 ± 0.22	37
270.000	44.41095 ± 0.00060	4.656 ± 0.094	15
260.000	44.4041 ± 0.0016	1.72 ± 0.19	33
250.000	44.39817 ± 0.00072	−1.27 ± 0.11	18
	June 1996		
349.868	44.46975 ± 0.00064	21.028 ± 0.092	14
325.046	44.45085 ± 0.00082	17.34 ± 0.16	14
300.117	44.4331 ± 0.0015	12.35 ± 0.28	26
275.103	44.41576 ± 0.00051	6.38 ± 0.15	18
250.161	44.3979 ± 0.0011	−1.12 ± 0.18	19
	May 1997		
320.000	44.4477 ± 0.0030	16.06 ± 0.56	41
300.111	44.4327 ± 0.0024	12.12 ± 0.58	31
280.121	44.41807 ± 0.00080	7.80 ± 0.18	9
	June 1996		
349.868	25.35386 ± 0.00054	21.92 ± 0.21	16
325.046	25.34225 ± 0.00058	17.19 ± 0.12	16
300.117	25.33223 ± 0.00042	12.65 ± 0.25	17
275.103	25.32191 ± 0.00064	6.51 ± 0.18	15
250.161	25.31168 ± 0.00056	−0.84 ± 0.15	18
	May 1997		
320.000	25.3392 ± 0.0011	16.45 ± 0.32	22
300.111	25.33100 ± 0.00062	12.92 ± 0.26	14
280.112	25.3221 ± 0.0012	7.28 ± 0.18	9

[a] The expanded ($k = 2$) uncertainties are listed for both $a(T, p = 0)$ and β_a.

with increasing pressure consistent with coupling of the radial gas modes with a predicted nonradial shell resonances.[38,39] The excess line width also increased with increasing pressure and confirmed the correct selection of mode (0, 5) for exclusion from the analysis. At $T = 300$ K in the 45 mm sphere $\Delta g/f$ for mode (0, 5) was $350 \cdot 10^{-6}$ at $p = 4$ MPa.

For the 45 mm resonator the (u/a) obtained from mode (0, 2) was lower than the $\langle u/a \rangle$, and the excess half widths were at all pressures about $200 \cdot 10^{-6}$, that is, a factor of 5 greater than for any other mode studied. At $T = 300$ K $\Delta g/f$ for the selected modes increased from about $3 \cdot 10^{-5}$ to $6 \cdot 10^{-5}$, and these variations with density were anticipated on the basis of results reported elsewhere.[39,40,44,45,71−73] Although no measurements were conducted to determine the source of these discrepancies, it is tempting to speculate that the excess losses and dispersion observed for (0, 2) arose from the slot around the equator terminated by a volume partially occupied by an O-ring that acted as a Helmholtz resonator, and based solely on this argument mode (0, 2) was eliminated from the regression.

Nevertheless, (u/a) that span $<10^{-5} \cdot u$ at a temperature and pressure were obtained from modes (0, 3) and (0, 4) for the 45 mm resonator and modes (0, 2) and (0, 3) for the 25 mm sphere. The span is taken as an estimate of the uncertainty in the measured u. The discussion now returns to consider the resonators $a(T, p = 0)$ and comparisons of the $\beta_a(T)$ with values reported in the literature.

The 1995 measurements with the 45 mm sphere extended to a pressure of 7 MPa, that is, at least a factor of 2 higher than that used for the measurements performed in both 1996 and

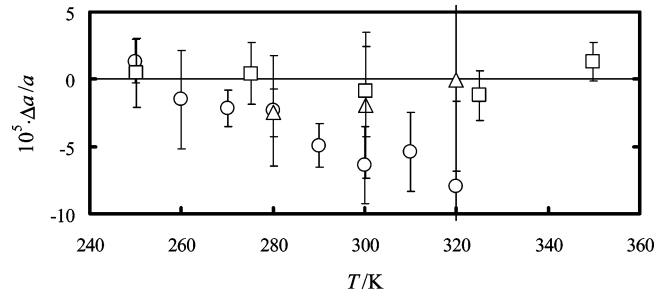

Figure 7. Deviations $\Delta a = \{a(\text{expt}) - a(\text{calc})\}$ of the measured radius a(expt) from the value obtained from the linear representation of the measurements obtained in 1996 and given by eq 8 with a(calc) for the sphere of the 45 mm nominal radius as a function of temperature T at $p = 0$. The error bars are the expanded ($k = 2$) uncertainty. ○, results obtained in 1995; □, results obtained in 1996; and △, results obtained in 1997 after relocating the equipment.

1997. For the 1995 measurements, the leading four terms of eq 3 were required to represent the results at each temperature over the whole pressure range, while the results from 1996 and 1997 required between three and four terms to accommodate the results. Therefore, the pressure range of each isotherm for all measurements was progressively truncated in the analysis with eq 3 to provide "best" three term expression and apparent third acoustic virial coefficients. Nevertheless, the values of $C_{p,m}^{pg}$ and β_a obtained by truncating the pressure range with either eqs 3 or 6 agreed within the combined standard deviations.[44]

In this analysis with eq 3 the (u/a) were weighted by the lesser of

$$(2 \cdot 10^{-6} f/\delta f)^2 \tag{7}$$

and unity, so that usually all measurements contributed equally. In eq 7, δf is the standard deviation of the measured frequency. The similarity of the fractional standard deviation for $\langle u/a \rangle^2$ for the selected modes at each pressure and the $(u/a)^2$ for the whole isotherm, listed in Table 1, suggests that eq 3 provided an adequate representation of the results.

Values of $a(T, p = 0)$ and β_a obtained from the regression analysis with the leading three terms of eq 2 of the (u/a) from the selected modes along each isotherm over a truncated pressure range are listed in Table 1.

The radius $a(T, p = 0)$ of the 45 mm resonator, determined from the 1996 data listed in Table 1, were represented by

$$a(T, p = 0)/\text{mm} = 44.4142[1 + 16.1414 \cdot 10^{-6}\{(T/\text{K}) - 273.15\}] \tag{8}$$

with a standard deviation $s(a)$ of 0.46 μm $\{s(a)/\langle a \rangle \approx 10^{-5}\}$ and shown in Figure 7 as a deviation from eq 8. The $a^{-1}(da/dT) = 16.14 \cdot 10^{-6}$ obtained from eq 8 was about 1 % below the literature value.[69] The $a(T, p = 0)$ obtained in 1997 differ from eq 8, as shown in Figure 7, by less than the expanded uncertainty assigned to each measurement. The 1995 determinations of $a(T, p = 0)$ show systematic deviations from eq 8 that increase with increasing temperature to lie up to $80 \cdot 10^{-6} \cdot a$ below at the highest temperature of 320 K, and there are two plausible sources for these variation. The first arises from a chemical impurity, such as water, that would introduce a systematic error in the speed of sound that increased with increasing temperature. However, no compositional analyses were performed to determine the presence of impurities, and this postulate is purely conjecture. The second proposed source of the difference in radius as a function of temperature arises from mechanical variations in the resonator between measurements. The transducer housings were removed after the 1995

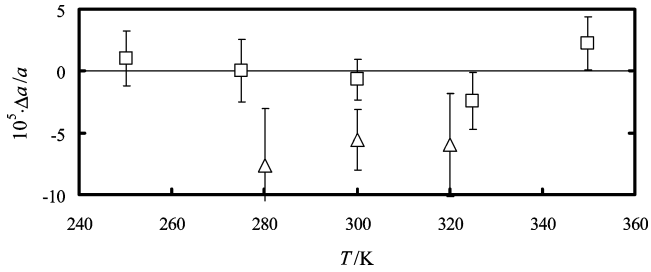

Figure 8. Deviations $\Delta a = \{a(\text{expt}) - a(\text{calc})\}$ of the measured radius a(expt) from the value obtained from the linear representation of the measurements obtained in 1996 and given by eq 9 with a(calc) for the sphere of the 25 mm nominal radius as a function of temperature T at $p = 0$. The error bars are the expanded ($k = 2$) uncertainty. □, results obtained in 1996; and △, results obtained in 1997 after relocating the equipment.

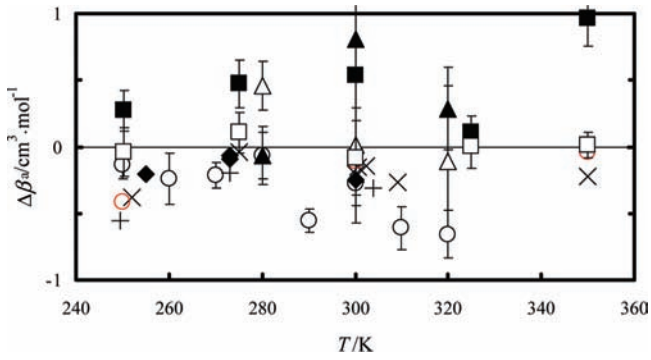

Figure 9. Deviations $\Delta\beta = \{\beta(\text{expt}) - \beta(\text{calc})\}$ of the measured second acoustic virial coefficient β(expt) from the value obtained from the linear representation of the measurements obtained in 1996 and given by eq 10 with β(calc) for the sphere of the 45 mm nominal radius as a function of temperature T. The error bars are the expanded ($k = 2$) uncertainty. ○, results obtained in 1995 for the sphere of the 45 mm nominal radius; □, results obtained in 1996 for the sphere of the 45 mm nominal radius; △, results obtained in 1997 after relocating the equipment for the sphere of the 45 mm nominal radius; ■, results obtained in 1996 for the sphere of the 25 mm nominal radius; ▲, results obtained in 1997 after relocating the equipment for the sphere of the 25 mm nominal radius; ◆, ref 39; ×, ref 45; +, ref 74; and red outline circle, ref 40.

measurements, modified, and relocated in this resonator wall. This process required removal of the housing from the extender, shown in Figure 3, and replacement of the silver O-ring between the resonator wall and the transducer housing. This might be expected to alter the average volume of the resonator and, therefore, the effective radius, but not the temperature dependence, leading to a systematic error. In the absence of other information we are unable to determine the source of this temperature dependent variation of the radius with time.

For the nominal 25 mm radius sphere the $a(T, p = 0)$ obtained in 1996 and listed in Table 1 are shown in Figure 8 as deviations from

$$a(T, p = 0)/\text{mm} = 25.3211[1 + 16.5818 \cdot 10^{-6}\{(T/\text{K}) - 273.15\}] \quad (9)$$

Equation 9 represented the $a(T, p = 0)$ with a standard deviation of 0.44 μm $\{100 \cdot s(a)/\langle a\rangle = 1.8 \cdot 10^{-5}\}$and gave $a^{-1}(\text{d}a/\text{d}T) = 16.58 \cdot 10^{-6}$, that is, 1.7 % greater than the literature value.[69] The radius determined in 1997 at temperatures of (300 and 320) K both lie about $50 \cdot 10^{-6} \cdot a$ below eq 9, while the value obtained at $T = 280$ K differs fractionally by $-74 \cdot 10^{-6}$ that corresponds to a variation of 0.01 % in the resonator's volume. These differences might arise from the removal and insertion of the transducers between 1996 and 1997.

The second acoustic virial coefficient β_a obtained in 1996 with the 45 mm radius sphere and listed in Table 1 are shown in Figure 9 as deviations from

$$\beta_a/\text{cm}^3 \cdot \text{mol}^{-1} = -9.8008 \cdot 10^{-4}\{(T/\text{K}) - 273.15\}^2 + 0.27425\{(T/\text{K}) - 273.15\} + 5.7438 \quad (10)$$

Equation 10 represented the measurements with a standard deviation $s(\beta_a)$ of about 0.07 cm^3·mol^{-1}, $\{100 \cdot s(\beta_a)/\langle\beta_a\rangle = 0.6\}$. The β_a obtained with the 45 mm radius sphere in 1995 and 1997 differ from eq 10, as shown in Figure 9, by $< \pm 0.5$ cm^3·mol^{-1} that are, except for the 1995 data at $T = 290$ K and $T = 310$ K, within less than 2.5 times the combined expanded uncertainty. The β_a determined from the 25 mm radius sphere lie within the combined expanded uncertainty of the values used to determine eq 10 except at $T = 350$ K where the difference is about three times the combined expanded error.

The β_a reported by other workers[39,40,45,74] are shown in Figure 9 as deviations from eq 10. The values of β_a reported Ewing and Goodwin[39] lie < 0.25 cm^3·mol^{-1} below eq 10, while those of Boyes[45] and Estrada-Alexanders and Trusler[40] deviate from eq 10 by less than -0.4 cm^3·mol^{-1} in the overlapping temperature range. The β_a reported by Ewing et al.[74] lie 0.3 cm^3·mol^{-1} below eq 10 at temperatures that overlap those of the 1996 measurements and by -0.5 cm^3·mol^{-1} when eq 10 is extrapolated to a temperature 0.73 K below the lowest temperature of (251.16 to 249.43) K.

The speeds of sound, listed in Table 2, were obtained from the mean $\langle u/a\rangle$ at each temperature and pressure, combined with $a(T, p)$, and are shown as relative factional deviations from the equation of state reported by Tegeler et al.[60] in Figures 10, 11, and 12. The uncertainty δu at a confidence interval of 0.95 ($k = 2$) for the 45 mm radius resonator is about $\pm$ 0.02 m·s^{-1} ($\delta u/u \approx \pm 5 \cdot 10^{-5}$), while for the 25 mm radius sphere $\delta u \approx \pm$ 0.03 m·s^{-1} ($\delta u/u < \pm 8 \cdot 10^{-5}$). These estimates of uncertainty were obtained by combining in quadrature contributions of $\delta u \approx \pm$ 0.003 m·s^{-1} for δa of the 45 mm radius sphere, $\delta u \approx \pm$ 0.006 m·s^{-1} for δa of the 25 mm radius sphere, agreement between the selected modes of $\delta u \approx \pm$ 0.003 m·s^{-1}, the uncertainty in the corrected frequency of $\delta u \approx \pm$ 0.003 m·s^{-1}, pressure where $|\delta u|$ varied from $\pm$ ($2.5 \cdot 10^{-5}$ to 0.003) m·s^{-1}, and temperature for which $\delta u \approx \pm$ 0.003 m·s^{-1} that were obtained with $(\partial u/\partial T)_p$ and $(\partial u/\partial p)_T$ estimated from ref 60. The uncertainty in the elastic constants, used to calculate both the ratio $\{a(T, p)/a(T, p = 0)\}$ and correction for coupling between the gas and the shell motion, contributes to δu which increases with pressure to reach about $\pm 10^{-5} \cdot u$ at $p = 7$ MPa.

The coefficients in the equation of state of Tegeler et al.[60] were determined, in part, from sound speed measurements independent of those reported here, including those obtained with spherical acoustic resonators and reported in refs 39, 40, and 45. The uncertainty in the estimated speed of sound was cited in ref 60 as $< \pm$ 0.02 %. The measurements reported by Boyes[45] at $p = 10$ MPa and $T = 252$ K lie, as shown in Figure 13, 0.012 % below the correlation of Tegeler et al.,[60] while the results reported by Estrada-Alexanders and Trusler[40] differ from ref 60 by $< \pm$ 0.004 % at temperatures that overlap the range covered in this work and pressures up to 19 MPa. At $T = 300$ K and $p < 7$ MPa the u reported by Ewing and Goodwin[39] deviate by $(-2 \text{ to } 3) \cdot 10^{-5} \cdot u$ from ref 60. Ewing and Goodwin[39] used a pressure compensated aluminum resonator, while both Estrada-Alexander and Trusler[40] and Boyes[45] used stainless steel spheres. The correction applied to the measured frequency for the elastic response of the shell is a function of the wall material and is about a factor of 3 greater for a resonator constructed

Table 2. Speed of Sound u as a Function of Temperature T and Pressure p Obtained with Both of the 45 mm and 25 mm Radius Spheres as a Function of Time

T	p	u	p	u	p	u
K	MPa	m·s^{-1}	MPa	m·s^{-1}	MPa	m·s^{-1}
			$a \approx 45$ mm			
			October 1995			
320.000	5.8199	341.243	4.4822	339.001	2.3331	335.852
	0.4505	333.627	0.3110	333.482	0.1805	333.349
310.000	6.5958	337.020	4.6246	333.589	2.3301	330.379
	0.4634	328.349	0.3292	328.225	0.1986	328.105
	0.1047	328.020				
300.000	6.5958	331.208	5.8329	329.796	4.6573	327.876
	2.3315	324.807	1.1809	323.609	0.3083	322.843
	0.1838	322.742	0.0305	322.616		
290.000	3.4778	320.364	2.3250	319.083	1.1916	318.037
	0.1964	317.297	0.0536	317.203		
280.000	6.6103	318.936	5.7670	317.479	4.6479	315.830
	2.3428	313.260	0.3283	311.827	0.2001	311.759
270.000	5.7752	311.124	4.6759	309.592	3.5218	308.292
	0.4672	306.205	0.3258	306.151	0.2000	306.108
	0.0532	306.055				
260.000	6.6023	305.842	4.6240	303.042	3.5075	301.947
	0.3273	300.368	0.1986	300.345		
250.000	5.8230	297.759	4.6529	296.356	2.3658	294.798
	0.3294	294.466	0.1980	294.473	0.0537	294.482
			$a \approx 45$ mm			
			June 1996			
349.868	2.7112	352.186	1.3977	350.238	0.8645	349.504
	0.7267	349.320	0.5945	349.144	0.4470	348.950
	0.3073	348.768	0.1829	348.607	0.0489	348.434
325.046	1.3765	337.358	0.8708	336.757	0.7360	336.603
	0.4386	336.267	0.3145	336.130	0.1929	335.997
	0.0481	335.835				
300.117	1.3786	323.871	0.8681	323.392	0.7299	323.270
	0.4455	323.023	0.3081	322.909	0.1930	322.814
	0.0481	322.692	1.3786	323.889	0.8682	323.405
275.103	1.3892	309.646	0.8602	309.334	0.7338	309.269
	0.8602	309.337	0.7062	309.255	0.5474	309.173
	0.3843	309.094	0.2069	309.012	0.0476	308.935
250.161	1.4011	294.624	0.7325	294.563	0.5986	294.561
	0.4477	294.560	0.3091	294.566	0.1920	294.572
	0.0487	294.574				
			May 1997			
320.000	1.5508	334.886	1.0539	334.304	0.5764	333.773
	0.1020	333.276				
300.111	1.0117	323.529	0.8680	323.391	0.7016	323.241
	0.5581	323.115	0.3954	322.976	0.2447	322.851
	0.1003	322.731				
280.121	1.8344	312.907	1.6017	312.723	1.3968	312.571
	1.1849	312.423	0.9646	312.277	0.7480	312.141
	0.5311	312.013	0.3077	311.887	0.0991	311.774
			$a \approx 25$ mm			
			June 1996			
349.868	1.3977	350.260	0.8646	349.5243	0.7267	349.340
	0.4470	348.966	0.3073	348.7836	0.1828	348.615
	0.0489	348.435				
325.046	2.7214	339.142	1.3766	337.3671	0.8708	336.763
	0.5927	336.443	0.4386	336.2665	0.3145	336.127
	0.1929	335.993				
300.117	1.3786	323.889	0.8682	323.4052	0.7299	323.280
	0.4455	323.033	0.3081	322.9103	0.1930	322.814
275.103	1.3893	309.667	0.8603	309.3457	0.7338	309.279
	0.5917	309.204	0.8602	309.3473	0.7062	309.264
	0.5474	309.180	0.3843	309.0978	0.2068	309.010
250.161	1.4011	294.651	0.8756	294.5830	0.7325	294.578
	0.5986	294.574	0.4477	294.5680	0.3091	294.569
	0.1920	294.575	0.0488	294.5752		
			May 1997			
320.000	1.5508	334.899	1.0539	334.316	0.5764	333.785
	0.1020	333.278				
300.111	1.8364	324.371	1.6180	324.143	1.1661	323.695
	0.9630	323.500	0.7391	323.296	0.5280	323.113
280.121	1.3964	312.580	0.9624	312.273	0.7458	312.132
	0.5294	312.003	0.3052	311.874		

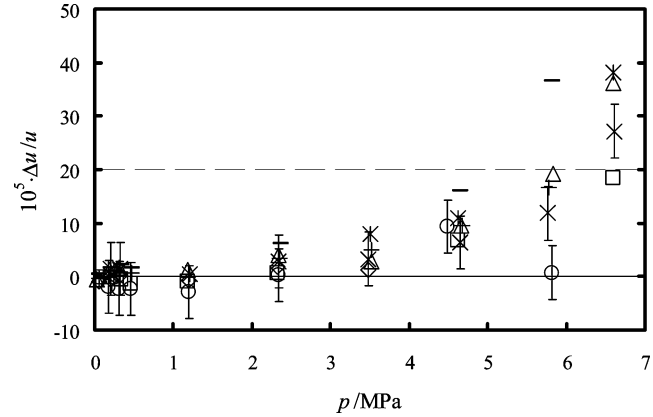

Figure 10. Relative deviations $\Delta u/u = \{u(\text{expt}) - u(\text{calc})\}/u(\text{calc})$ of the sound speed determined in 1995 with the 45 mm sphere with u(expt) listed in Table 2 from the equation of state of ref 60 and u(calc) as a function of pressure p. —, $T = 250$ K; *, $T = 260$ K; +, $T = 270$ K; ×, $T = 280$ K; ◇, $T = 290$ K; △, $T = 300$ K; □, $T = 310$ K; ○, $T = 320$ K. The error bars, shown solely for the isotherm $T = 320$ K for the purpose of clarity, illustrate the typical expanded uncertainty ($k = 2$). The dashed line at $\Delta u/u = 20 \cdot 10^{-5}$ is the uncertainty in u obtained from the equation of state.[60]

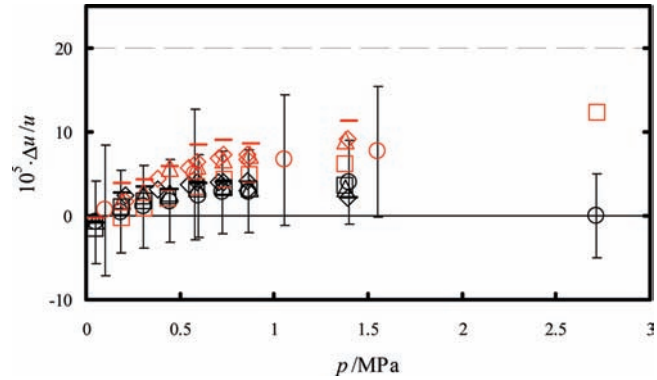

Figure 11. Relative deviations $\Delta u/u = \{u(\text{expt}) - u(\text{calc})\}/u(\text{calc})$ of the sound speed determined in 1996 with both the 25 mm and the 45 mm spheres with u(expt) listed in Table 2 from the equation of state of ref 60 and u(calc) as a function of pressure p. Deviations for the 45 mm radius sphere: —, $T = 250$ K; ◇, $T = 275$ K; △, $T = 300$ K; □, $T = 325$ K; ○, $T = 350$ K. Deviations for the 25 mm radius sphere: red dash, $T = 250$ K; red outlined diamond, $T = 275$ K; red outlined triangle, $T = 300$ K; red outlined square, $T = 325$ K; red outlined circle, $T = 349$ K. The error bars, shown solely for the isotherm $T = 350$ K for the purpose of clarity, illustrate the typical expanded uncertainty ($k = 2$). The dashed line at $\Delta u/u = 20 \cdot 10^{-5}$ is the uncertainty in u obtained from the equation of state.[60]

from aluminum when compared with a stainless steel sphere of the same dimensions.

In view of the agreement of about $\pm 5 \cdot 10^{-5} \cdot u$, shown in Figure 13, between independent sound speed measurements[39,40,45] with both each other and the equation of state of Tegeler et al.[60] and the estimated expanded ($k = 2$) uncertainty for the results listed in Table 2 of between $\pm(5 \text{ and } 8) \cdot 10^{-5} \cdot u$, further consideration is now given to the comparisons of the measured u, shown in Figures 10, 11, and 12, with estimates determined from ref 60.

The sound speed measurements obtained with the 45 mm sphere in 1995 extend to a maximum pressure of about 7 MPa, that is, at least 2.6 times that used for the results obtained in both 1996 and 1997. At all temperatures studied that include the temperature range of (250 to 320) K and $p < 2.5$ MPa the 1995 determinations of u deviate, as Figure 10 shows, by $< \pm 5 \cdot 10^{-5} \cdot u$ from ref 60 and within the expanded uncertainty assigned to the measurements and in agreement with those

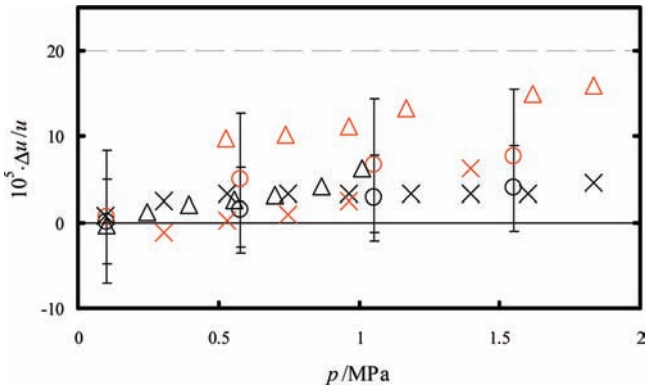

Figure 12. Relative deviations $\Delta u/u = \{u(\text{expt}) - u(\text{calc})\}/u(\text{calc})$ of the sound speed determined in 1997 with both the 25 mm and the 45 mm spheres with u(expt) listed in Table 2 from the equation of state of ref 60 and u(calc) as a function of pressure p. Deviations for the 45 mm radius sphere: ×, $T = 280$ K; △, $T = 300$ K; ○, $T = 320$ K. Deviations for the 25 mm radius sphere: red cross, $T = 280$ K; red outlined triangle, $T = 300$ K; red outlined circle, $T = 320$ K. The error bars, shown solely for the isotherm $T = 320$ K for the purpose of clarity, illustrate the typical expanded uncertainty ($k = 2$). The dashed line at $\Delta u/u = 20 \cdot 10^{-5}$ is the uncertainty of the u obtained from the equation of state.[60]

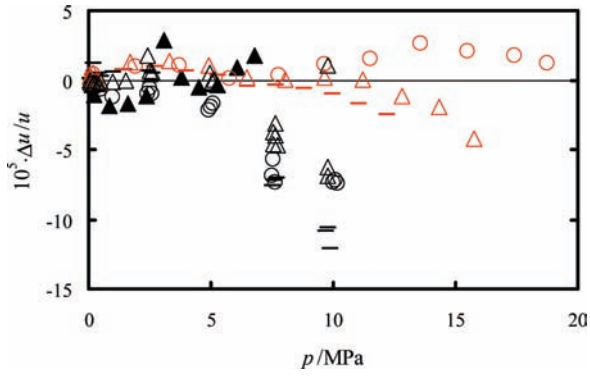

Figure 13. Relative deviations $\Delta u = u(\text{expt}) - u(\text{calc})$ of the sound speed reported by other workers with u(expt) from that of the equation of state of ref 60 and u(calc) as a function of pressure p. —, $T = 251$ K, ref 45; △, $T = 300$ K, ref 45; ○, $T = 350$ K, ref 40; ▲, $T = 300$ K, ref 39; orange outlined triangle, $T = 304$ K, ref 74; red dash, $T = 250$ K, ref 40; red outlined triangle, $T = 300$ K, ref 40; and red outlined circle, $T = 350$ K, ref 40. The uncertainty of the u obtained from the equation of state was $\Delta u/u = \pm 20 \cdot 10^{-5}$.[60]

reported in refs 39, 40, and 45. However, at $p > 2.5$ MPa the $\Delta u/u$ increases with increasing pressure systematically, albeit without obvious temperature dependence, to lie, at $p \approx 6.8$ MPa, $4 \cdot 10^{-4} \cdot u$ from ref 60. These differences cannot be explained by a constant variation in chemical purity between the sources of argon used. These differences could be accounted for with a fractional uncertainty in pressure of 0.005, albeit highly unlikely. The correction for shell motion and the compliance $a^{-1}(\partial a/\partial p)_T$ used to determine $a(T, p)$ both require the elastic constants for stainless steel, but even at $p = 7$ MPa the shell motion correction is equivalent to the observed difference in the speed of sound of $4 \cdot 10^{-4} \cdot u$ and the adjustment for compliance $<10^{-5} \cdot a$ so that errors in the elastic constants cannot be the source of the observed difference. No experiments were performed to determine the source of the observed differences in $u(p)$, and it is speculated they arose because the practical resonator, shown in Figures 1 and 2, did not comply with the assumptions used to obtain the correction for shell motion of an isotropic spherical cavity.[27,37]

Alternative means of determining $a(T, p)$ {and $a(T, p = 0)$} are provided by dialatometry,[38] pycnometry,[75] and dimensional microwave measurements,[76−81] including the use of quasi-spherical cavities to remove the degeneracy of the electromagnetic modes[82−84] when operated with a gas of known complex relative electric permittivity such as He.[85]

The speed of sound obtained in 1996 extended to a maximum pressure of 2.7 MPa and the u, as shown in Figure 12, from both the 25 mm and the 45 mm radius resonators agree within the estimated expanded uncertainty, albeit with differences from ref 60 that increase with increasing pressure to be $<10^{-4} \cdot u$ at $p = 2.7$ MPa. The sound speeds determined in 1997, which extended to a maximum pressure of 1.8 MPa, from both resonators are also in agreement within the expanded uncertainty with similar deviations from ref 60 that are shown in Figure 12 and consistent with the estimated expanded uncertainty.

Literature Cited

(1) Jaeschke, M.; Humphreys, A. E. Standard GERG Virial Equation for Field Use and GERG Technical Monograph TM5 (1991). *Forsch. Ber. VDI, Reihe 6*, *266*, **1992**.

(2) Jaeschke, M.; Schley, P.; Janssen-van Rosmalen, R. Thermodynamics Research Improves Energy Measurement in Natural Gas. *Int. J. Thermophys.* **2002**, *23*, 1013–1031.

(3) GERG, the European Gas Research Group. http://www.gerg.info/.

(4) Moldover, M. R.; Buckley, T. J. Reference Values of the Dielectric Constant of Natural Gas Components Determined with a Cross Capacitor. *Int. J. Thermophys.* **2001**, *22*, 859–885.

(5) Goodwin, A. R. H. *Phase Boundary Data for Natural Gas Mixtures*, Gas Research Institute: Chicago, IL, 1994; Report number 94/0499.

(6) Goodwin, A. R. H. *Phase Boundary Data for Natural Gas Mixtures*, Gas Research Institute: Chicago, IL, 1997.

(7) Goodwin, A. R. H.; Hill, J. A.; Savidge, J. L. Acoustic measurements in natural gas mixtures. *Proc. Int. Gas Res. Conf.*; Dolenc, D. A., Ed.; **1995**, *1*, 681.

(8) Goodwin, A. R. H.; Hill, J. A.; Savidge, J. L. Detection of phase boundaries for natural gas mixtures. *Proc. Int. Gas Res. Conf.*; Dolenc, D. A., Ed.; **1995**, *1*, 667.

(9) Goodwin, A. R. H.; Trusler, J. P. M. *Sound Speed in Experimental Thermodynamics Volume VI: Measurement of the Thermodynamic Properties of Single Phases*; Goodwin, A. R. H., Marsh, K. N., Wakeham, W. A., Eds.; Elsevier Science: Amsterdam, 2003; Chapter 6.

(10) Trusler, J. P. M.; Zarari, M. The speed of sound and derived thermodynamic properties of methane at temperatures between 275 and 375 K and pressures up to 10 MPa. *J. Chem. Thermodyn.* **1992**, *24*, 973–991.

(11) Wakeham, W. A.; Assael, M. A.; Atkinson, J. S.; Bilek, J.; Fareleira, M. N. A.; Fitt, A. D.; Goodwin, A. R. H.; Oliveira, C. M. B. P. Thermophysical Property Measurements: The Journey from Accuracy to Fitness for Purpose. *Int. J. Thermophys.* **2007**, *28*, 372–416.

(12) Mehl, J. B.; Moldover, M. R. Precondensation phenomena in acoustic measurements. *J. Chem. Phys.* **1982**, *77*, 455–465.

(13) Fawcett, D. Ph.D. Thesis, Murdoch University, Australia, 1995.

(14) Edwards, T. J.; Pack, D. J.; Fawcet, D.; Trengove, R. D.; Resuggan, M. *Measurement and Prediction of Speed of Sound with Application to Gas Flow Metering in Australian Natural Gas, Minerals and Energy Research*; Report No. 150; Institute of Western Australia: Perth, Australia, 1995.

(15) Moldover, M. R.; Marsh, K. N.; Barthel, J.; Buchner, R. Relative Permittivity and Refractive Index. In *Experimental Thermodynamics Vol. VI, Measurement of the Thermodynamic Properties of Single Phases*; Goodwin, A. R. H., Marsh, K. N., Wakeham, W. A., Eds.; Elsevier: Amsterdam, The Netherlands, 2003; Chapter 9, p 127−235.

(16) Goodwin, A. R. H.; Mehl, J. B.; Moldover, M. R. Reentrant radio-frequency resonator for automated phase-equilibria and dielectric measurements in fluids. *Rev. Sci. Instrum.* **1996**, *67*, 4294–4303.

(17) Goodwin, A. R. H.; Moldover, M. R. Phase border and density determinations in the critical region of (carbon dioxide + ethane) determined from dielectric permittivity measurements. *J. Chem. Thermodyn.* **1997**, *29*, 1481–1494.

(18) Kandil, M. E.; Marsh, K. N.; Goodwin, A. R. H. A re-entrant resonator for the measurement of phase borders: dew pressures for {0.4026 CH_4 + 0.5974 C_3H_8}. *J. Chem. Thermodyn.* **2005**, *37*, 684–691.

(19) Kandil, M. E.; Marsh, K. N.; Goodwin, A. R. H. Determination of the relative permittivity and density within the gas phase and liquid volume fraction formed obtained within the two phase region for {0.4026 CH_4 + 0.5974 C_3H_8} with a radio frequency re-entrant cavity. *J. Chem. Eng. Data* **2007**, *52*, 1660–1671.

(20) Kandil, M. E.; Marsh, K. N.; Goodwin, A. R. H. Determination of the relative permittivity, ε', of methylbenzene at temperatures between (290 and 406) K and pressures below 20 MPa with a radio frequency re-entrant cavity and evaluation of a MEMS capacitor for the measurement of ε'. *J. Chem. Eng. Data* **2008**, *53*, 1056–1065.

(21) May, E. F.; Edwards, T. J.; Mann, A. G.; Edwards, C. Dew point, liquid volume, and dielectric constant measurements in a vapor mixture of methane + propane using a microwave apparatus. *Int. J. Thermophys.* **2003**, *24*, 1509–1525.

(22) Moldover, M. R.; Gillis, K. A.; Hurly, J. J.; Mehl, J. B.; Wilhelm, J. Acoustic Measurements in Gases: Applications to Thermodynamic Properties, Transport Properties, and the Temperature Scale. In *Handbook of Elastic Properties of Solids, Liquids, and Gases, Volume IV, Elastic Properties of Fluids: Liquids and Gases*, Levy, M., Bass, H. E., Stern, R. R. Eds.-in-chief; Levy, M., Raspet, R., Sinha, D., Vol. Eds.; Furr, L., tech. Ed.; Keppens, V., supervising Ed.; Academic Press: New York, 2001; Chapter 12.

(23) Moldover, M. R.; Waxman, M.; Greenspan, M. Spherical acoustic resonators for temperature and thermophysical property measurements. *High Temp. High Press.* **1979**, *11*, 75–86.

(24) Moldover, M. R.; Mehl, J. B. Precision acoustic measurements with a spherical resonator: Ar and C_2H_4. *J. Chem. Phys.* **1981**, *74*, 4062–4077.

(25) Mehl, J. B. Moldover, M. R. Specific heat and virial coefficient measurements with a spherical acoustic resonator. In *Proc. Eighth Symp. on Thermophysical Properties, Vol. 1: Thermophysical Properties of Fluids*; Sengers, J. V., Ed.; The American Society of Mechanical Engineers: New York, 1982; p 134.

(26) Moldover, M. R.; Mehl, J. B. Precision Measurements and Fundamental Constants II. *Natl. Bur. Stand., Spec. Pub.*; Taylor, B. N., Phillips, W. D., Eds.; *617*, **1984**; p 281.

(27) Moldover, M. R.; Mehl, J. B.; Greenspan, M. Gas-filled spherical resonators: Theory and experiment. *J. Acoust. Soc. Am.* **1986**, *79*, 253–272.

(28) Mehl, J. B.; Moldover, M. R. Measurement of the ratio of the speed of sound to the speed of light. *Phys. Rev. A* **1986**, *34*, 3341–3344.

(29) Trusler, J. P. M. *Physical Acoustics and Metrology of Fluids*; Adam-Hilger: Bristol, 1991.

(30) Goodwin, A. R. H. Trusler, J. P. M. Sound Speed and Heat Capacity of Gases. In *Heat Capacities of Liquids and Vapours*; Letcher, T. J., Ed.; Royal Society of Chemistry: Cambridge, 2009.

(31) Colgate, S. O.; Sivaraman, A.; Reed, K. R. *Acoustic Determination of the Thermodynamic Reference State Heat Capacity of n-Heptane Vapor*; Report RR-109; Gas Processors Association: Tulsa, OK, 1987.

(32) Mehl, J. B. Acoustic resonance frequencies of deformed spherical resonators. *J. Acoust. Soc. Am.* **1982**, *71*, 1109–1113.

(33) Mehl, J. B. Acoustic resonance frequencies of deformed spherical resonators. II. *J. Acoust. Soc. Am.* **1986**, *79*, 278–285.

(34) Ewing, M. B.; Goodwin, A. R. H. Thermophysical properties of alkanes from speeds of sound determined using a spherical resonator 4. 2-Methylpropane at temperatures in the range 251 to 320 K and pressures in the range 5 to 114 kPa. *J. Chem. Thermodyn.* **1991**, *23*, 1107–1120.

(35) Ewing, M. B.; Goodwin, A. R. H. Thermophysical properties of alkanes from speeds of sound determined using a spherical resonator 5. 2-Methylbutane at temperatures in the range 260 to 320 K and pressures in the range 2.8 to 80.9 kPa. *J. Chem. Thermodyn.* **1992**, *24*, 301–315.

(36) Ewing, M. B.; McGlashan, M. L.; Trusler, J. P. M. The Temperature-Jump Effect and the Theory of the Thermal Boundary Layer for a Spherical Resonator. Speeds of Sound in Argon at 273.16 K. *Metrologia* **1986**, *22*, 93–102.

(37) Mehl, J. B. Spherical acoustic resonator: Effects of shell motion. *J. Acoust. Soc. Am.* **1985**, *78*, 782–788.

(38) Moldover, M. R.; Trusler, J. P. M.; Edwards, T. J.; Mehl, J. B.; Davis, R. S. Measurement Of The Universal Gas-Constant R Using a Spherical Acoustic Resonator. *J. Res. Nat. Bur. Stand.* **1988**, *93*, 85–144.

(39) Ewing, M. B.; Goodwin, A. R. H. An apparatus based on a spherical resonator for measuring the speed of sound in gases at high pressures. Result for argon at temperatures between 255 and 300 K and at pressure up to 7 MPa. *J. Chem. Thermodyn.* **1992**, *24*, 531–547.

(40) Estrada-Alexanders, A. F.; Trusler, J. P. M. The Speed of Sound in Gaseous Argon at Temperatures between 110 and 450 K and at pressure up to 19 MPa. *J. Chem. Thermodyn.* **1995**, *27*, 1075–1089.

(41) Trusler, J. P. M. Unpublished calculations of the acoustic admittance of slits reported in ref 38.

(42) Ewing, M. B.; Trusler, J. P. M. Speeds of sound in CF_4 between 175 and 300 K measured with a spherical resonator. *J. Chem. Phys.* **1989**, *90*, 1106–1115.

(43) Ewing, M. B.; Trusler, J. P. M. Interaction second virial coefficients of (N_2 + Ar) between 90 and 373 K. *Physica A* **1992**, *184*, 437–450.

(44) Trusler, J. P. M.; Zarari, M. P. Second and third acoustic virial coefficients of methane at temperatures between 014 and 264 K. *J. Chem. Thermodyn.* **1995**, *27*, 771–778.

(45) Boyes, S. J. Ph.D. Thesis, University of London, 1992.

(46) Fawcett, D. Ph.D. Thesis, Murdoch University, Australia, 1995.

(47) Hill, J. A.; Goodwin, A. R. H. *Electrostatic transducers and methods of manufacturing the same*. U.S. Patent 5,600,610, February 4, 1997.

(48) Hill, J. A.; Goodwin, A. R. H. *Electrostatic transducers and methods of manufacturing the same*. U.S. Patent 5,745438, April 28, 1998.

(49) Ruska, W. E. A.; Hurt, L. J.; Kobayashi, R. Circulating Pump for High Pressure and−200 to +400 C Application. *Rev. Sci. Instrum.* **1970**, *41*, 1444–1446.

(50) Mansoorian, H.; Capps, E. F.; Gielen, H. L.; Eubank, P. T.; Hall, K. R. Compact, magnetic recirculating pump for wide-range temperature and pressure operation. *Rev. Sci. Instrum.* **1975**, *46*, 1350–1351.

(51) Ziger, D. H.; Eckert, C. A. Simple high-pressure magnetic pump. *Rev. Sci. Instrum.* **1982**, *53*, 1296–1297.

(52) Rogers, W. J.; Fontalba, F.; Capps, E. F.; Holste, J. C.; Marsh, K. N.; Hall, K. R. Magnetic circulating pumps for use over wide ranges of temperature and pressure. *Rev. Sci. Instrum.* **1988**, *59*, 193–194.

(53) Peleties, F.; Trusler, J. P. M.; Goodwin, A. R. H.; Maitland, G. C. Circulating Pump for High-Pressure and High-Temperature Applications. *Rev. Sci. Instrum.* **2005**, *76*, 105103.

(54) http://www.navcen.uscg.gov/Loran/default.htm.

(55) Horowitz, P.; Hill, W. *The art of electronics*, Cambridge University Press: New York, 1986, p 250.

(56) Trusler, J. P. M. Ph.D. Thesis, University of London, 1984.

(57) Mehl, J. B. Analysis of resonance standing-wave measurements. *J. Acoust. Soc. Am.* **1978**, *64*, 1523–1525.

(58) Ewing, M. B.; Trusler, J. P. M. On the analysis of acoustic resonance measurement. *J. Acoust. Soc. Am.* **1989**, *85*, 1780–1782.

(59) Lemmon, E. W.; McLinden, M. O.; Huber, M. L. *REFerence fluid PROPerties program 23*, version 7.1; Physical and Chemical Properties Division National Institute of Standards and Technology: Boulder, CO.

(60) Tegeler, Ch.; Span, R.; Wagner, W. A New Equation of State for Argon Covering the Fluid Region for Temperatures from the Melting Line to 700 K at Pressures up to 1000 MPa. *J. Phys. Chem. Ref. Data* **1999**, *28*, 779–850.

(61) Preston-Thomas, H. The International Temperature Scale of 1990 (ITS-90). *Metrologia* **1990**, *27*, 3–10.

(62) McGlashan, M. L. The International Temperature Scale of 1990 (ITS-90). *J. Chem. Thermodyn.* **1990**, *22*, 653–663.

(63) Wieser, M. E. Atomic Weights Of The Elements 2005 (IUPAC Technical Report). *Pure Appl. Chem.* **2006**, *78*, 2051–2066.

(64) Mohr, P. J.; Taylor, B. N.; Newell, D. B. CODATA recommended values of the fundamental physical constants: 2006. *J. Phys. Chem. Ref. Data* **2008**, *37*, 1187–1284.

(65) Lemmon, E. W.; Jacobsen, R. T. Viscosity and Thermal Conductivity Equations for Nitrogen, Oxygen, Argon, and Air. *Int. J. Thermophys.* **2004**, *25*, 21–69.

(66) Ledbetter, H. M. Stainless-steel elastic constants at low temperature. *J. Appl. Phys.* **1981**, *52*, 1587–1589.

(67) Varshni, Y. P. Temperature dependence of the elastic constants. *Phys. Rev. B* **1970**, *2*, 3952–3958.

(68) Ledbetter, H. M. Temperature behaviour of Young's moduli of forty engineering alloys. *Cryogenics* **1982**, *22*, 653–656.

(69) Curruccini, R. J.; Gniewek, J. J. Thermal expansion of technical solids at low temperature. *NBS Monogr. 29 (U.S.)* **1961**, 11.

(70) Kroger, F. R.; Swenson, C. A. Absolute linear thermal-expansion measurements on copper and aluminum. *J. Appl. Phys.* **1977**, *48*, 853–864.

(71) Ewing, M. B.; Goodwin, A. R. H. Speeds of sound, perfect gas heat capacities and acoustic virial coefficients for methane determined using a spherical resonator at temperatures between 255 and 300 K and pressures in the range 171 kPa to 7.1 MPa. *J. Chem. Thermodyn.* **1992**, *24*, 1257–1274.

(72) Ewing, M. B.; Goodwin, A. R. H. Speeds of sound, perfect-gas heat capacity, and second acoustic virial coefficient for air at the temperature 255 K and pressures in the range 0.031 to 6.9 MPa. *J. Chem. Thermodyn.* **1993**, *25*, 423–427.

(73) Ewing, M. B.; Goodwin, A. R. H. Speeds of sound for a natural gas of specified composition at the temperature 255 K and pressures in the range 0.031 to 6.9 MPa. *J. Chem. Thermodyn.* **1993**, *25*, 1503–1511.

(74) Ewing, M. B.; Owusu, A. A.; Trusler, J. P. M. Second Acoustic Virial Coefficients of Argon Between 100 and 304 K. *Physica A* **1989**, *156*, 899–908.

(75) Goodwin, A. R. H.; Bradsell, C. H.; Toczylkin, L. S. (p, ρ, T) of liquid n-octane obtained with a spherical pycnometer at temperatures of 298.03 and 313.15 K and pressures in the range 0.7 to 32 MPa. *J. Chem. Thermodyn.* **1996**, *28*, 637.

(76) Moldover, M. R.; Boyes, S. J.; Meyer, C. W.; Goodwin, A. R. H. Thermodynamic Temperatures of the Triple Points of Mercury and

Gallium and in the Interval 217 to 303 K. *J. Res. Nat. Inst. Stand. Tech.* **1999**, *104*, 11–46.

(77) Ewing, M. B.; Trusler, J. P. M. Primary acoustic thermometry between $T = 90$ K and $T = 300$ K. *J. Chem. Thermodyn.* **2000**, *32*, 1229–1255.

(78) Gallop, J. C.; Radcliffe, W. J. Dimensional measurement by microwave resonances. *J. Phys. E: Sci. Instrum.* **1981**, *14*, 461–463.

(79) Dominique, J.; Gallop, J. C.; Radciffe, W. J. A microwave method for thermal expansion measurement. *J. Phys. E: Sci. Instrum.* **1983**, *16*, 1200–1202.

(80) Gallop, J. C.; Radcliffe, W. J. Shape and dimensional measurement using microwaves. *J. Phys. E: Sci. Instrum.* **1986**, *19*, 413–416.

(81) Ewing, M. B.; Mehl, J. B.; Moldover, M. R.; Trusler, J. P. M. Microwave Measurements of the Thermal Expansion of a Spherical Cavity. *Metrologia* **1988**, *25*, 211–220.

(82) May, E. F.; Pitre, L.; Mehl, J. B.; Moldover, M. R.; Schmidt, J. W. Quasi-spherical cavity resonators for metrology based on the relative dielectric permittivity of gases. *Rev. Sci. Instrum.* **2004**, *75*, 3307–3317.

(83) Mehl, J. B.; Moldover, M. R.; Pitre, L. Designing quasi-spherical resonators for acoustic thermometry. *Metrologia* **2004**, *41*, 295–304.

(84) Pitre, L.; Moldover, M. R.; Tew, W. L. Acoustic thermometry: new results from 273 to 77 K and progress towards 4 K. *Metrologia* **2006**, *43*, 142–162.

(85) Hurly, J. J.; Moldover, M. R. Ab Initio Values of the Thermophysical Properties of Helium as Standards. *J. Res. Natl. Inst. Stand. Technol.* **2000**, *105*, 667–688.

Received for review May 14, 2009. Accepted July 13, 2009. The work reported was sponsored by the Gas Research Institute (GRI) contract number 5093-260-2599 entitled *Phase Boundary Data for Natural Gas Mixtures* and conducted between 1993 and 1998 under the direction of Jeffrey Savidge, Senior Project Manager. In 2000, GRI merged with the Institute of Gas Technology (IGT) to create a company known by the acronym GTI. Approval to publish this work was granted by GTI as one of the remaining business matters of GRI.

JE900428G